SANDIA REPORT
SAND2000-1018
Unlimited Release
Printed April 2000

Grating Light Reflection Spectroelectrochemistry for Detection of Trace Amounts of Aromatic Hydrocarbons in Water

M. J. Kelly, W. C. Sweatt, S. A. Kemme, K. J. Kasunic, D. S. Blair, S. H. Zaidi, J. R. McNeil, L. W. Burgess, A. M. Brodsky, and S. A. Smith

Prepared by
Sandia National Laboratories
Albuquerque, New Mexico 87185 and Livermore, California 94550

Sandia is a multiprogram laboratory operated by Sandia Corporation, a Lockheed Martin Company, for the United States Department of Energy under Contract DE-AC04-94AL85000.

Sandia National Laboratories

Issued by Sandia National Laboratories, operated for the United States Department of Energy by Sandia Corporation.

Available to DOE and DOE contractors from
Office of Scientific and Technical Information
P.O. Box 62
Oak Ridge, TN 37831

Prices available from (703) 605-6000
Web site: http://www.ntis.gov/ordering.htm

Available to the public from
National Technical Information Service
U.S. Department of Commerce
5285 Port Royal Rd
Springfield, VA 22161

DISCLAIMER

Portions of this document may be illegible in electronic image products. Images are produced from the best available original document.

SAND2000-1018
Unlimited Release
Printed April 2000

Grating Light Reflection Spectroelectrochemistry for Detection of Trace Amounts of Aromatic Hydrocarbons in Water

M. J. Kelly
Information Detection, Extraction, and Analysis Department

W. C. Sweatt, S. A. Kemme, and K. J. Kasunic[a]
Photonics and Microfabrication Department

D. S. Blair
Systems Analysis Department I

Sandia National Laboratories
P.O. Box 5800
Albuquerque, NM 87185-0343

[a]*Current address: Department of Mathematics, University of Arizona, Tucson, AZ*

S. H. Zaidi and J. R. McNeil
Center for High Technology Materials
University of New Mexico
Albuquerque, NM

L. W. Burgess, A. M. Brodsky, and S. A. Smith
Center for Process Analytical Chemistry
University of Washington
Seattle, WA

Abstract

Grating light reflection spectroscopy (GLRS) is an emerging technique for spectroscopic analysis and sensing. A transmission diffraction grating is placed in contact with the sample to be analyzed, and an incident light beam is directed onto the grating. At certain angles of incidence, some of the diffracted orders are transformed from traveling waves to evanescent waves. This occurs at a specific wavelength that is a function of the grating period and the complex index of refraction of the sample. The intensities of diffracted orders are also dependent on the sample's complex index of refraction. We describe the use of GLRS, in combination with electrochemical modulation of the

grating, for the detection of trace amounts of aromatic hydrocarbons. The diffraction grating consisted of chromium lines on a fused silica substrate. The depth of the grating lines was 1 μm, the grating period was 1 μm, and the duty cycle was 50%. Since chromium was not suitable for electrochemical modulation of the analyte concentration, a 200 nm gold layer was deposited over the entire grating. This gold layer slightly degraded the transmission of the grating, but provided satisfactory optical transparency for the spectroelectrochemical experiments. The grating was configured as the working electrode in an electrochemical cell containing water plus trace amounts of the aromatic hydrocarbon analytes. The grating was then electrochemically modulated *via* cyclic voltammetry waveforms, and the normalized intensity of the zero order reflection was simultaneously measured. We discuss the lower limits of detection (LLD) for two analytes, 7-dimethylamino-1,2-benzophenoxazine ("Meldola's Blue" dye) and 2,4,6-trinitrotoluene (TNT), probed with an incident HeNe laser beam (λ = 543.5 nm) at an incident angle of 52.5°. The LLD for 7-dimethylamino-1,2-benzophenoxazine is approximately 50 parts per billion (ppb), while the LLD for TNT is approximately 50 parts per million (ppm). The possible factors contributing to the differences in LLD for these analytes are discussed. This is the final report for a Sandia National Laboratories Laboratory Directed Research and Development (LDRD) project conducted during fiscal years 1998 and 1999 (case number 3518.190).

Table of Contents

Introduction

Current drinking water standards specify that concentrations of certain aromatic hydrocarbons must be very low, e.g., below 100 parts per billion (ppb). However, quantitation of compounds in water at these concentrations can be difficult and is typically performed using purge-and-trap analytical methods. These techniques have inherently long analysis times and, for field-deployable instrumentation, high device maintenance requirements and equipment failure rates. The goal of this research was to provide the technology base for eventual production of a field-deployable sensor that provides the ability to measure aromatic hydrocarbons in water at concentrations as low as 100 ppb.

The technology we developed uses spectroelectrochemistry as its fundamental transduction mechanism. Here, the detection and quantitation of analytes in water rely on monitoring the electrochemical generation or consumption of an optically detectable compound. The spectroscopic method that we are combining with electrochemistry is known as grating light reflection spectroscopy (GLRS). A new and emerging technology [1-3], it noninvasively provides information about the complex index of refraction of a sample. This can then be translated into quantitative chemical information. Briefly, a transmission diffraction grating is placed in contact with the sample to be analyzed, and an incident light beam is directed onto the grating. Some of the diffracted orders are transformed from traveling waves to evanescent waves at a specific wavelength and angle of incidence, both of which are functions of the grating period and the complex index of refraction of the sample. The intensities of some reflected orders are also strongly dependent on the sample's complex index of refraction. In our method, we use these reflected intensities as the analytical signal.

The redistribution of intensity from the evanescent wave into reflected light will depend upon the dielectric properties of the sample. These properties include the refractive index and the absorption index (a quantity related to the molar extinction coefficient). The relationship between these parameters can be expressed by the following equation for the complex index of refraction (n^*):

$$n^* = n - ik \qquad \{1\}$$

where n is denoted as the real part of the complex refractive index, and k is the absorption index (referred to as the imaginary part of the refractive index). Since these parameters are related to each other by a complex function, they will induce nearly orthogonal responses in the reflection spectrum, and these can be independently quantitated. However, refraction and absorption do influence each other due to a phenomenon called anomalous dispersion, which causes the refractive index to become anamolously low on the low wavelength side of an absorbance band, and anomalously high on the high wavelength side of the band. This feature will induce further changes in the appearance of the singularity around an absorbance band.

The relative merits of GLRS with respect to related techniques for measurement of small changes in the complex index of refraction was the subject of extensive theoretical study by this LDRD project team, but will not be discussed in the main body of this report. Much of that work has been published [4] in a peer-reviewed journal, wherein the relative sensitivities of total internal reflection (TIR) techniques (cf. Refs. 5-9) and surface plasmon resonance (SPR) approaches (cf. Refs. 10-12) were numerically simulated. Reference 4 is attached as Appendix I of this report, and serves as a summary of the theoretical aspect of the project. Similarly, a great deal of numerical simulation work was performed to determine optimal grating properties and experimental GLRS configurations. This work is also not included herein. Rather, we focus here on the experimental effort aimed at a laboratory demonstration of the grating light reflection spectroelectrochemical sensor concept. This focus is appropriate because the experimental program encompassed all of the major milestones and deliverables outlined in the original LDRD proposal. Our experiments have shown that grating light reflection spectroelectrochemistry is indeed a sensitive method for detection of trace levels of aromatic hydrocarbons in water.

We performed the evaluations of our laboratory prototype using two aromatic hydrocarbons: 7-dimethylamino-1,2-benzophenoxazine ("Meldola's Blue" dye) and 2,4,6-trinitrotoluene (TNT). Meldola's Blue was chosen as a model for analytes that are known to exhibit large changes in optical absorbance upon electrochemical conversion to an oxidized or reduced form of the molecule. TNT was chosen for two reasons. First, there is currently a great deal of interest at Sandia (and elsewhere) in the development of methods for detection of explosive molecules at trace levels. Second, in contrast to Meldola's Blue, TNT does not have high optical absorbance at the wavelength of our spectroelectrochemistry experiments (543.5 nm). We therefore considered this to be a useful way to begin to evaluate the sensitivity of grating light reflection spectroelectrochemistry for changes in the real part of the refractive index.

In the remainder of this report, we describe the details of our grating light reflection spectroelectrochemical experiments. The grating was configured as the working electrode in an electrochemical cell containing water plus trace amounts of the aromatic hydrocarbon analytes. The grating was electrochemically modulated *via* cyclic voltammetry waveforms, and the normalized intensity of the zero reflected order was simultaneously measured. We discuss the lower limits of detection (LLD) for the two analytes and present hypotheses for the dramatic differences in their spectroelectrochemical behavior.

Experimental

We designed and fabricated a spectroelectrochemical cell and optical spectroscopy system (see Figure 1), and used them to evaluate the prototype grating light reflection spectroelectrochemical sensor concept. The electrochemical cell, fabricated by Manufacturing Processing Department 1481 at Sandia, was constructed of high-density polyethylene (HDPE). The cell had a capacity of approximately 1.4 mL. The HDPE formed three sides of the cell cavity, and the fourth side of the cell was enclosed by a removable diffraction grating. A channel machined into the front face of the

cell was designed to hold an elastomeric o-ring, and the grating was pressed against the o-ring with nylon screws. This ensured a liquid-tight seal. The cell's working electrode was a diffraction grating with chromium metal lines deposited onto a 1 cm x 2 cm fused silica substrate. The depth of the grating lines was 1 μm, the grating period was 1 μm, and the duty cycle was 50%. The grating was manufactured (Photronics Inc., Brookfield, CT) by etching the blanket chromium layer using typical processes for production of photomasks. A continuously conductive region around the perimeter of the grating was used to make electrical contact with the grating lines. Spring-loaded, gold-plated pogo pins (Newark Electronics, Gaffney, SC) were installed in the cell body and were used to make electrical contact to the continuously conductive region of the grating. Since chromium is not a suitable working electrode for electrochemical measurements, approximately 200 nm of semi-conformal gold was evaporated over the entire grating (Figure 1a). This gold layer slightly degraded the transmission of the grating, but provided satisfactory optical transparency for the spectroelectrochemical experiments. The counter electrode was a platinum coil, and a silver wire was used as a pseudo-reference electrode ("Ag RE").

A Bioanalytical Systems (West Lafayette, IN) model BAS 100B/W potentiostat and a personal computer were used to control the electrochemical modulation of the diffraction grating. In various experiments, we performed potential step, cyclic voltammetry (CV), and Osteryoung square wave voltammetry (OSWV) to electrochemically modulate the potential of the grating with respect to the pseudo-reference electrode.

The electrochemical cell was mounted on one of two high-precision rotation stages (from Newport Corporation, Irvine, CA, or Polytec PI, Physik Instrumente, Auburn, MA). A linear traveling stage (Newport) was mounted directly onto the rotation stage and was used to align the grating directly along the axis of rotation. The linear stage was also mounted perpendicular to the plane of the grating to ensure that the location of the beam on the grating would not change when the angle of incidence was changed.

The GLRS measurements (see schematic, Figure 1c) were made at a fixed angle of 52.5±0.2°, which is at or near the spectral singularity, i.e., the angle at which the first transmitted diffraction order changes from propagating to evanescent (according to Braggs' diffraction equation). The light source was a green HeNe laser (Melles Griot, Rochester, NY) operating at 543.5 nm. The laser beam was positioned in a TM polarization configuration (i.e., the E field was in the plane of incidence of the grating). The laser beam was directed through a chopper wheel (Stanford Research Systems, Sunnyvale, CA) operating at about 190 Hz. The beam was steered by two plane mirrors through a beam pickoff wedge (New Focus, Inc., Santa Clara, CA) onto the grating. The pickoff was directed through an iris onto a silicon photodiode detector. The zero diffracted order (reflection, from the beam incident upon the grating) was directed through an iris onto a second silicon photodiode detector. The current outputs from the detectors were sent to two transimpedance amplifiers, and the resulting voltage signals were sent to two digital lock-in amplifiers (Stanford Research Systems, Sunnyvale, CA). A custom LabView® (National

Instruments, Austin, TX) virtual instrument, controlled by a personal computer, was used to control the motion of the rotation stage and to acquire the data from the lock-in amplifiers. In this report, all experimental data shown are the ratios of the zero order reflectance intensity divided by the beam pickoff reference intensity. This was performed to compensate for fluctuations in laser power.

Meldola's Blue dye was obtained from Aldrich Chemical Co. (Milwaukee, WI). TNT was obtained as a 90 parts per million (ppm) solution in deionized water from Materials Characterization Department 1822 at Sandia. Spectroelectrochemistry experiments were performed either in high-performance liquid chromatography (HPLC) grade water (Fisher Scientific, Pittsburgh, PA) or in a supporting electrolyte of 0.05 M potassium nitrate (KNO_3, Hi Pure Grade, Spex, Metuchen, NJ) in HPLC-grade water. The absence of a supporting electrolyte in the former case would typically result in unacceptably high solution resistivity; however, Meldola's Blue (an ionic dye) imparted sufficient conductance to the water to allow electrochemical modulation of the grating. In some experiments, the solutions were sparged with high-purity nitrogen (boil-off from a liquid nitrogen reservoir) to remove dissolved oxygen.

Prior to performing electrochemical and GLRS experiments with the electrochemical cell depicted in Figure 1b, the electrochemistry of Meldola's Blue and TNT were first characterized in a conventional electrochemical cell with a volume of approximately 10 mL. The working electrode was a gold disk (A = 0.03 cm^2), the counter electrode was a platinum coil, and a silver wire was used as a pseudo-reference electrode ("Ag RE"). The electrochemistry of the two analytes was characterized by CV and/or OSWV. The purpose of these experiments was to compare the electrochemical performance characteristics of the cell in Figure 1b to those of a conventional cell. This comparison allowed us to assess the effects of non-conventional electrochemical cell designs that were necessary in order to combine electrochemistry and GLRS.

Results

Meldola's Blue – Electrochemistry

In Figure 2, the cyclic voltammogram of Meldola's Blue in 0.1 M KNO_3 is shown. This experiment was performed in a conventional electrochemical cell with a gold disk working electrode. In this figure, as well as other figures that depict the electrochemical behavior of the analytes, a background voltammogram (0.1 M KNO_3 supporting electrolyte in this case) is shown for comparison. Two voltammetric peaks are significant here. First, as the potential of the working electrode was scanned in the cathodic (negative) direction, a peak was observed at approximately –350 mV vs. Ag RE due to the reduction of Meldola's Blue:

$$MB^+ + H^+ + 2e^- \rightarrow MBH \qquad \{2\}$$

Upon reversal of the scan direction, a peak was observed during the anodic (positive) scan at approximately –200 mV due to the oxidation of the reduced form of Meldola's Blue:

$$MBH \rightarrow MB^{+} + H^{+} + 2e^{-} \quad \{3\}$$

The increased sharpness and amplitude of the oxidation peak (compared to the reduction peak) suggests that the reduced form of Meldola's Blue strongly adsorbs to the surface of the gold working electrode. The adsorbed species is then desorbed during the anodic scan when the electrochemical overpotential is sufficient to provide the thermodynamic driving force for reaction 3.

In Figure 3, another cyclic voltammogram of Meldola's Blue in 0.1 M KNO_3 is shown. This experiment was performed in the GLRS electrochemical cell with the Au/Cr/fused silica grating working electrode. Reduction and oxidation peaks corresponding to reactions 2 and 3 are observed at approximately –300 and –250 mV vs. Ag RE, respectively, although they are not as sharp as the corresponding peaks in Figure 2. There are several probable reasons that the electrochemistry of Meldola's Blue is not as well defined with this cell configuration. First, we did not polish the conformal gold coating on the grating prior to cyclic voltammetry, whereas this was routinely performed with the gold disk electrode of Figure 2. A polishing step typically removes surface contamination that can deleteriously affect the kinetics of electron transfer reactions at electrodes, resulting in broad voltammetric peaks. We did not polish the grating because it was likely that such a step would irreparably damage it and make it useless for further experiments. Second, electrical contact to the active portion of the grating (i.e., that portion of the grating in contact with the solution) was made *via* a point contact to the continuously conductive region of the grating. We suspect that contact resistance (in the pogo pin to gold layer contact) and/or sheet resistance (in the conductive regions of the grating) contributed to an uncompensated iR (i.e., current x resistance) decrease in the magnitude of the working electrode potential with respect to the pseudo-reference electrode. The net result is that the actual magnitude of the working electrode potential is smaller than that displayed in the voltammogram. Even with the differences noted between Figures 2 and 3, we concluded that our GLRS electrochemical cell was entirely adequate for spectroelectrochemistry experiments.

In Figure 4, the cyclic voltammogram of Meldola's Blue in water is shown. This experiment was performed in a conventional electrochemical cell with a gold disk working electrode. A reduction peak for reaction 2 is observed at approximately –350 mV vs. Ag RE, and the oxidation peak for reaction 3 occurs at approximately +100 mV vs. Ag RE. It is somewhat unusual to perform cyclic voltammetry in water without a supporting electrolyte (e.g., a salt like KNO_3) to impart conductivity. However, Meldola's Blue is ionic [13] and as seen by comparison of Figures 2 and 4, imparts sufficient conductance to water to allow satisfactory control of the working electrode potential in the absence of a supporting electrolyte.

In Figure 5, another cyclic voltammogram of Meldola's Blue in water is shown. This experiment was performed in the GLRS electrochemical cell with the Au/Cr/fused silica grating working electrode. Reduction peaks corresponding to reaction 2 are observed between approximately –800 and –2100 mV vs. Ag RE, while oxidation current corresponding to reaction 3 is observed in the

vicinity of +2500 mV vs. Ag RE. Several features of these voltammograms should be noted. First, the Meldola's Blue peaks are very broad, poorly defined, and occur at high potentials. We suspect that the main contributors to these effects are the same factors noted previously in the discussion for Figure 3, as well as the high resistivity (> 10 MΩ-cm) of the HPLC-grade water. Second, even though the working electrode is scanned to cathodic and anodic potentials far in excess of the potential for water electrolysis, we do not see evidence for water electrolysis in the background scan. This is presumably due to a large uncompensated iR effect, which results in the actual magnitude of the working electrode potential being smaller than that displayed in the voltammogram. Even with the large differences noted between Figures 4 and 5, we concluded that our GLRS electrochemical cell was satisfactory for spectroelectrochemistry experiments on Meldola's Blue dye in water. We considered measurements in water to be a relevant test of the grating light reflection spectroelectrochemical sensor concept, in that it probed the usefulness of the technique for possible field use in detection of trace contaminants in water without the need for addition of analytical reagents.

Meldola's Blue – Grating Light Reflection Spectroelectrochemistry

The electrochemical reduction of Meldola's Blue is accompanied by large changes in the optical properties of the molecule [13]. In Figure 6, the optical absorbance spectrum of Meldola's Blue is compared to that of the reduced form of the molecule. This figure was adapted from reference 13. Meldola's Blue has a high absorption index (molar extinction coefficient = 22,700 $M^{-1}cm^{-1}$ at 568 nm), while the reduced form of the molecule is essentially optically transparent. Also note in Figure 6 that the difference in optical properties between the oxidized and reduced forms of the molecule is significant at the wavelength of our experiments (543.5 nm).

In Figure 7, the normalized zero order reflectance is shown as a function of time for CV experiments on a 2.7 ppm solution of Meldola's Blue in water, as well as for pure water. The grating was scanned between +3 and -3 volts at a scan rate of 500 mV/s. As noted, earlier, these potentials were not sufficient to electrolyze water, but were large enough to produce measurable changes in the reduction (and subsequent oxidation) currents attributable to the analyte. This modulation of the grating produced changes in the zero order reflectance that we fit to the following expression:

$$R = m1 + m2*[\sin(m3*t + m4)] \qquad \{4\}$$

In equation 4, t is time and m1, m2, m3, and m4 are fitting parameters. In Figure 7, the experimental data are represented by the symbols, while the sine curve fits are shown as the solid and dashed curves. The amplitude of the modulated reflectance is given by m2, which we refer to as the modulation coefficient. The offset of the zero order reflectance is given by m1. It is apparent from this figure that electrochemical modulation produces changes in reflectance characteristics that can be used to measure this analyte with excellent sensitivity.

In Figure 8, the modulation coefficient is shown as a function of Meldola's Blue dye concentration for a series of experiments analogous to that shown in Figure 7. In this figure (as well as subsequent figures of this type), the "control" experiment was conducted in an identical manner as the "dye" experiment (solution preparation, time, data acquisition/processing, etc.), obviously in the absence of any dye. In Figure 8, it can be seen that the electrochemically modulated zero order reflectance amplitude provides a sensitive measure of the dye concentration over a very large dynamic range.

Figure 9 is an expanded version of the results from Figure 8, and shows that sub ppm detection limits for the dye can be realized by this method. The lower limit of detection (LLD) can be estimated based on the concentration that produces the first significant response above the control value. Significance is determined by the precision of the measurements of the modulation coefficient. The control experiment in Figure 9 indicates that the modulation coefficient can be measured with an approximate uncertainty of ± 0.002. Adopting the convention that a signal-to-noise ratio of three is required for statistical significance, we consider a 0.006 increase in the modulation coefficient to be a reasonable estimate of the smallest meaningful change. In Figure 9, this occurs at a Meldola's Blue concentration of approximately 0.05 ppm (50 ppb).

In Figures 10 and 11, the values of m1 for experiments with Meldola's Blue are shown. Clearly, the offset of the modulated zero order reflectance also shows that a large linear dynamic range (Figure 10) and an excellent LLD (Figure 11) can be achieved by determination of this reflectance quantity. However, the drift in the control sample experiment may make this approach less attractive for analytical purposes.

In Figures 12 and 13, the zero order reflectance in the absence of electrochemical modulation are shown. For both the "dye" and the "control" experiments, this data was acquired immediately before (dye – open squares; control – x's) and immediately after (dye – open circles; control – open diamonds) the 4-cycle electrochemical modulation. Immediately before the electrochemical modulation, the grating was at rest potential. Immediately after the electrochemical modulation, the grating was in the process of returning to a rest potential from the final potential (+3 volts vs. the pseudo-reference electrode). Here, even in the absence of electrochemical modulation, the zero order reflectance changes in a useful manner as the dye concentration is changed. However, as with the plots of m1 (Figures 10 and 11), the drift in the control sample experiment may make this a less useful analytical measurement than determination of concentration *via* the electrochemical modulation coefficient (m2).

TNT – Electrochemistry

The voltammetric behavior of 2, 4, 6-trinitrotoluene (TNT) on some working electrodes (e.g., glassy carbon) has been reported to be characterized by 3 distinct peaks, corresponding to sequential reduction of the three nitro groups [14]:

$$TNT + e^- \rightarrow TNT^- \qquad \{5\}$$

$$TNT^{-} + e^{-} \rightarrow TNT^{2-} \quad \{6\}$$

$$TNT^{2-} + e^{-} \rightarrow TNT^{3-} \quad \{7\}$$

However, voltammetry of TNT on gold working electrodes is different. Although TNT has excellent electroactivity on gold at moderate cathodic potentials, distinct peaks are not observed for each of the three reduction reactions [14]. In Figure 14, the Osteryoung square wave voltammogram of TNT in 0.05 M KNO_3 is shown. This experiment was performed in a conventional electrochemical cell with a gold disk working electrode. Two distinct peaks are observed in this cathodic scan (at approximately –600 mV and –750 mV vs. Ag RE), and a third peak at approximately –350 mV vs. Ag RE may be present as well. These peaks presumably encompass some or all of reactions 5 – 7.

In Figure 15, another voltammogram of TNT in 0.05 M KNO_3 is shown. This experiment was performed in the GLRS electrochemical cell with the Au/Cr/fused silica grating working electrode. As expected, the peaks are broad and poorly-defined (for the reasons noted previously). However, our main interest in the voltammetry of TNT on the grating electrode was to determine if TNT had sufficient electroactivity to allow us to probe it by grating light reflection spectroelectrochemistry. For this purpose, the electrochemical reaction rate characterized by the cathodic current in Figure 15 was considered satisfactory to test this concept. Therefore, even with the rather large differences between Figures 14 and 15, we concluded that our GLRS electrochemical cell was satisfactory for spectroelectrochemistry experiments on TNT in 0.05 M KNO_3. It should be noted that the potassium nitrate supporting electrolyte was necessary to impart sufficient conductivity to the solution to allow reduction of TNT (and subsequent oxidation to form the neutral molecule) at reasonable potentials.

TNT - Grating Light Reflection Spectroelectrochemistry

In contrast to Meldola's Blue, TNT does not have high optical absorptivity at the wavelength of interest in these experiments (543.5 nm). In fact, the absorbance spectrum of TNT is characterized by a maximum that appears in the ultraviolet portion of the spectrum, typically below 250 nm. Further, the optical absorbance at 543.5 nm of reduced forms of TNT has, to our knowledge, not appeared in the literature, nor was it measurable with our experimental setup. Therefore, we do not know if reduction of TNT is accompanied by a change in optical absorbance, as was the case with Meldola's Blue (which was "bleached" *via* electrochemical reduction). However, the electrochemical reduction of TNT is undoubtedly accompanied by a change in the real part of the refractive index. Therefore, grating light reflection spectroelectrochemistry experiments on TNT were considered to be a first step to begin to evaluate the sensitivity of grating light reflection spectroelectrochemistry for changes in the real part of the refractive index.

In Figure 16, the zero order reflectance is shown as a function of time for CV experiments on a 45 ppm solution of TNT in 0.05 M KNO_3 (squares), as well as for pure 0.05 M KNO_3 (circles). Here, the grating was scanned between 0 and –1 volts at a scan rate of 100 mV/s. Comparison of

Figures 7 and 16 allows one to first conclude that the sensitivity and LLD for TNT are significantly worse than those for Meldola's Blue dye. In fact, we estimate the LLD for TNT to be on the order of 50 ppm, or roughly three orders of magnitude worse than for Meldola's Blue. This estimate resulted from an analysis similar to that described previously for approximating the LLD of Meldola's Blue. Also note that the amplitude of the modulated reflectance in Figure 16 is smaller for the 45 ppm TNT solution than for the blank solution. This is different from the results for Meldola's Blue, where increases in analyte concentration resulted in an increase in the modulated reflectance amplitude. The reasons for the different behavior of these two analytes remain under investigation. Our current hypothesis is that a large change in optical absorbance at 543.5 nm does not result from the electrochemical reduction of TNT (and subsequent oxidation back to the neutral molecule), and that grating light reflection spectroelectrochemistry under these conditions (543.5 nm light incident on a 1.0 μm period grating at 52.5°) is not a sensitive measure of the change in the real part of the refractive index that accompanies TNT reduction. Further, we hypothesize that the large decrease in optical absorbance at 543.5 nm that accompanies the electrochemical reduction of Meldola's Blue [13] is the principal reason it can be sensitively measured by grating light reflection spectroelectrochemistry under these conditions.

Conclusions

Our results show that the grating light reflection spectroelectrochemical approach to the analysis of Meldola's Blue in water provides good sensitivity and excellent lower limits of detection (less than 50 ppb). However, sensitivity and LLD for TNT analysis is significantly worse. The reason for this dramatic difference in detection limits is currently under investigation. Our working hypothesis is that the large decrease in optical absorbance (at 543.5 nm) that accompanies the electrochemical reduction of Meldola's Blue is reflected in a correspondingly large change in the measured complex index of refraction. We further hypothesize that no such change in optical absorbance at 543.5 nm accompanies the electrochemical reduction of TNT, and that grating light reflection spectroelectrochemistry under our experimental conditions (543.5 nm light incident on a 1.0 μm period grating at 52.5°) is not a sensitive measure of the change in the real part of the refractive index that accompanies TNT reduction. Changing the experiment to incorporate a broadband light source would increase the measurement's sensitivity to refractive index changes. This is because intensity redistributions in the spectral region of the singularity (especially those due to the presence of an analyte absorbance band) are not symmetrical with respect to wavelength. Thus a single wavelength measurement, such as that performed using a laser source, cannot guarantee that these changes are being accurately and/or sensitively monitored. A broadband measurement would allow the overall form of the reflectivity in the region of the critical wavelength to be mapped out, such that slight shifts in its position could be quantitated *via* fitting the spectral response to an ideal curve. However, even this will not maximize the technique's sensitivity unless the measurement is done within a wavelength region where the sample contains an absorbance band. For example, the TNT experiment could be reproduced with a 500 nm grating

at an incident angle of 56° to place the singularity at 250 nm and thus in the region of maximum absorbance for TNT, where the maximal singularity intensity redistribution would be observed.

Acknowledgments

Sandia is a multiprogram laboratory operated by Sandia Corporation, a Lockheed Martin company, for the U.S. Department of Energy under contract number DE-AC04-94AL85000. This work was funded by the Laboratory Directed Research and Development Program at Sandia from October 1, 1997 to September 30, 1999. Funding support from the Office of Naval Research is also gratefully acknowledged.

References

1. B. B. Anderson, A. M. Brodsky, and L. W. Burgess, "Grating Light Reflection Spectroscopy for Determination of Bulk Refractive Index and Absorbance", *Anal. Chem.* **68(7)**, 1081-1088 (1996).
2. B. B. Anderson, "Grating Light Reflection Spectroscopy", *Ph.D. Dissertation Thesis, University of Washington* (1996).
3. A. M. Brodsky, L. W. Burgess, and S. A. Smith, "Grating Light Reflection Spectroscopy", *Applied Spectroscopy*, **52(9)**, 332A-343A (1998).
4. K. J. Kasunic, "Comparison of Kretschmann-Raether Angular Regimes for Measuring Changes in Bulk Refractive Index", *Applied Optics*, **39(1)**, 61-64 (2000).
5. Y. Shi, A. F. Slaterbeck, C. J. Seliskar, and W. R. Heineman, "Spectroelectrochemical Sensing Based on Multimode Selectivity Simultaneously Achievable in a Single Device. 1. Demonstration of a Concept with Ferricyanide", *Anal. Chem.* **69(18)**, 3679-3686 (1997).
6. Y. Shi, C. J. Seliskar, and W. R. Heineman, "Spectroelectrochemical Sensing Based on Multimode Selectivity Simultaneously Achievable in a Single Device. 2. Demonstration of Selectivity in the Presence of Direct Interferences", *Anal. Chem.* **69(23)**, 4819-4827 (1997).
7. A. F. Slaterbeck, T. H. Ridgway, C. J. Seliskar, and W. R. Heineman, "Spectroelectrochemical Sensing Based on Multimode Selectivity Simultaneously Achievable in a Single Device. 3. Effect of Signal Averaging on Limit of Detection", *Anal. Chem.* **71(6)**, 1196-1203 (1999).
8. L. Gao, C. J. Seliskar, and W. R. Heineman, "Spectroelectrochemical Sensing Based on Multimode Selectivity Simultaneously Achievable in a Single Device. 4. Sensing with Poly(vinyl alcohol)-Polyelectrolyte Blend Modified Optically Transparent Electrodes", *Anal. Chem.* **71(18)**, 4061-4068 (1999).
9. Y. Shi, A. F. Slaterbeck, S. Aryal, C. J. Seliskar, W. R. Heineman, T. H. Ridgway, and J. H. Nevin, "New Spectroelectrochemical Sensor", *Proceedings of Micro- and Nanofabricated Structures and Devices for Biomedical Environmental Applications, Progress in Biomedical Optics*, January 26-27, 1998, San Jose, CA; P. L. Gourley and A. Katzir, Eds., **3258**, 56-65 (1998).
10. H. Kano and S. Kawata, "Grating-Coupled Surface Plasmon for Measuring the Refractive Index of a Liquid Sample", *Jpn. J. Appl. Phys.*, **34**, 331-335 (1995).
11. J. Homola, "Surface Plasmon Resonance Sensors: A Review", *Sensors and Actuators B: Chemical*, **54(1-2)**, 3-15 (1999).
12. A. H. Ali and C. A. Foss, Jr., "Electrochemically Induced Shifts in the Plasmon Resonance Bands of Nanoscopic Gold Particles Adsorbed on Transparent Electrodes", *J. Electrochem. Soc.*, **146(2)**, 628-636 (1999).

13. B. L. Ramos, S. J. Choquette, and G. Nagy, "Electrochemical Modulation of a Waveguide Interferometer", *Electroanalysis*, **12(2)**, 140-146 (2000).

14. A. Hilmi, J. H. T. Luong, and A.-L. Nguyen, "Development of Electrokinetic Capillary Electrophoresis Equipped with Amperometric Detection for Analysis of Explosive Compounds", *Anal. Chem.* **71(4)**, 873-878 (1999).

Figures

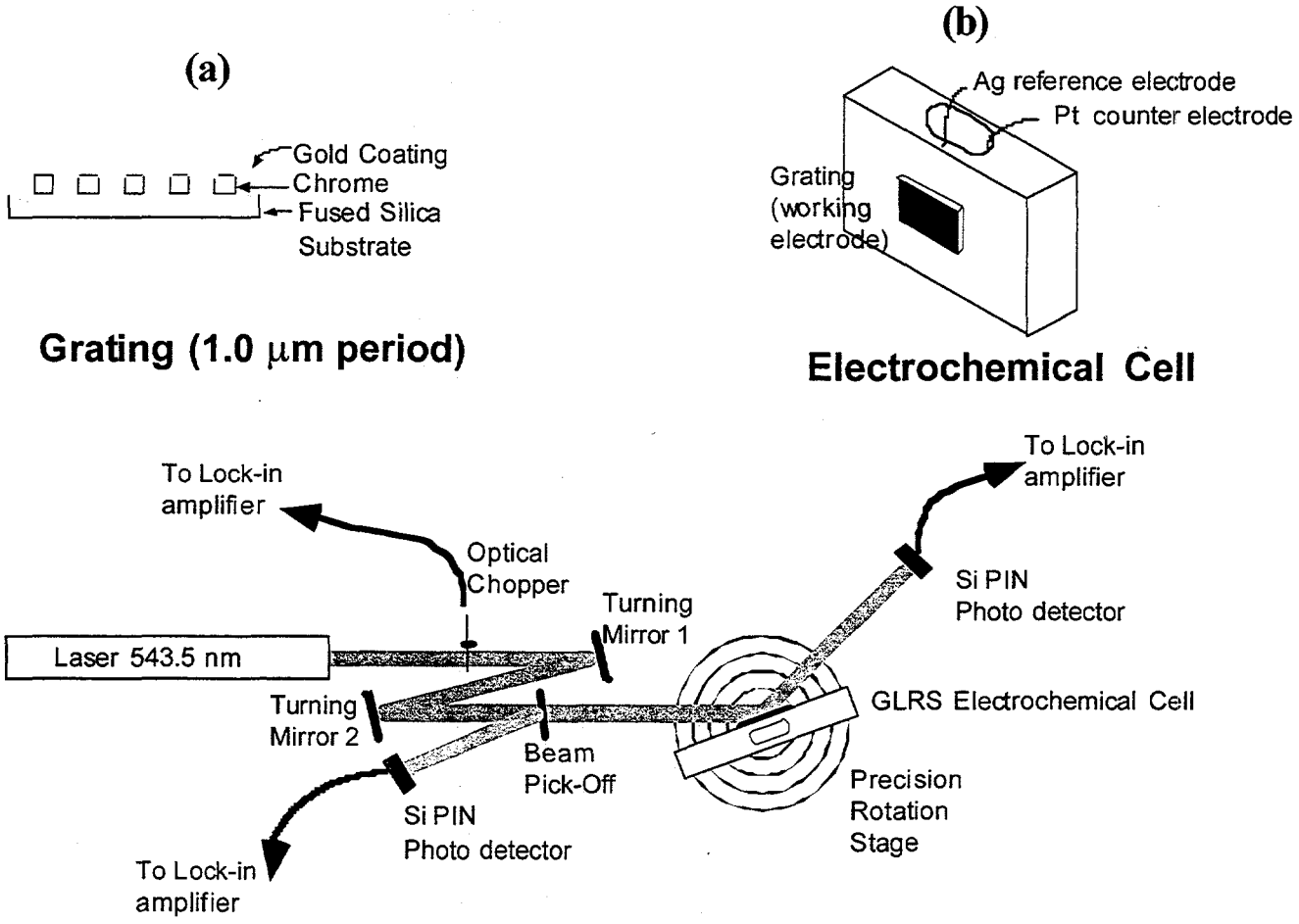

Figure 1. Grating Light Reflection Spectroelectrochemistry experiment. (a) Diffraction grating, 1.0 μm period, chromium on fused silica. A semi-conformal gold layer, approximately 200 nm thick, was deposited over the grating to improve electrochemical performance. (b) Three-electrode electrochemical cell. A liquid-tight seal between the grating and the high-density polyethylene cell body was achieved with an o-ring gasket. (c) Optical layout (see text for details).

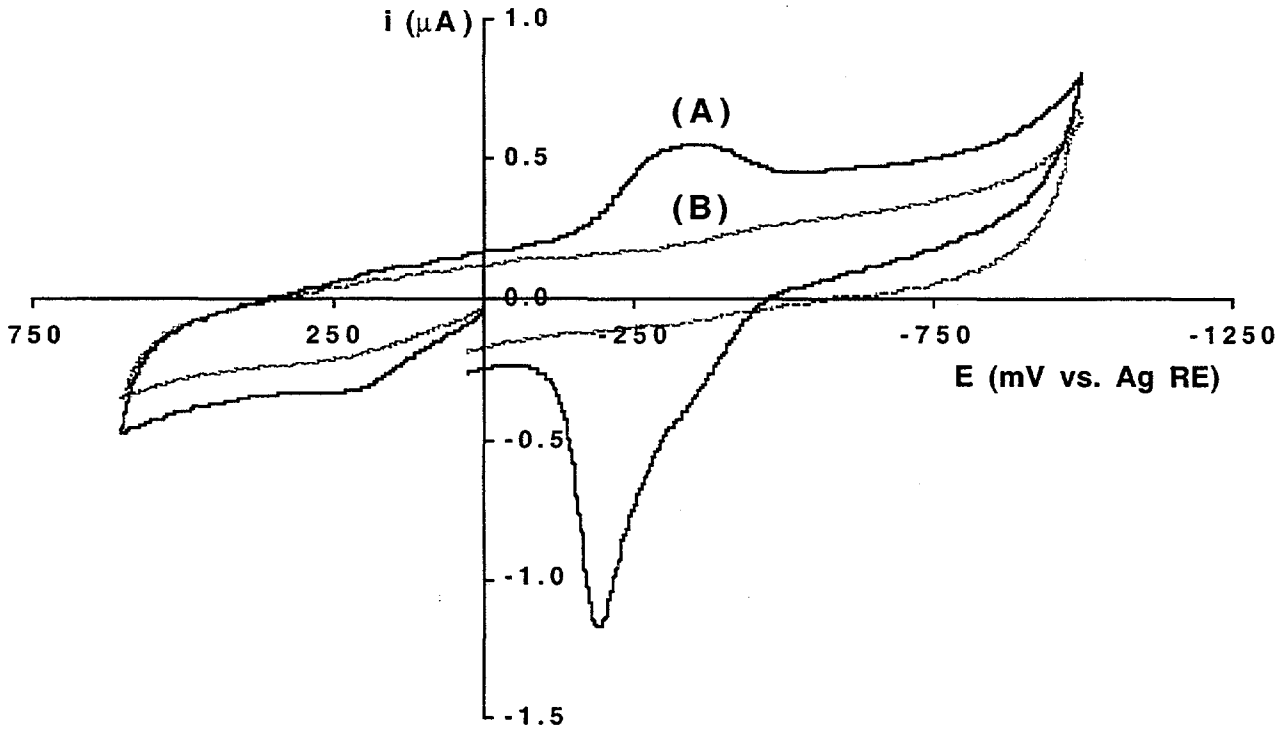

Figure 2. Cyclic voltammetry of Meldola's Blue in 0.1 M KNO_3, in a conventional electrochemical cell. Working electrode: 0.03 cm^2 gold disk. Dark curve (A) is 31 ppm Meldola's Blue. Light curve (B) is 0.1 M KNO_3 background. Initial potential: 0 mV vs. silver pseudo-reference electrode. Switching potentials: +600 and –1000 mV. Final potential: ~ 0 mV. Scan rate: 50 mV/sec.

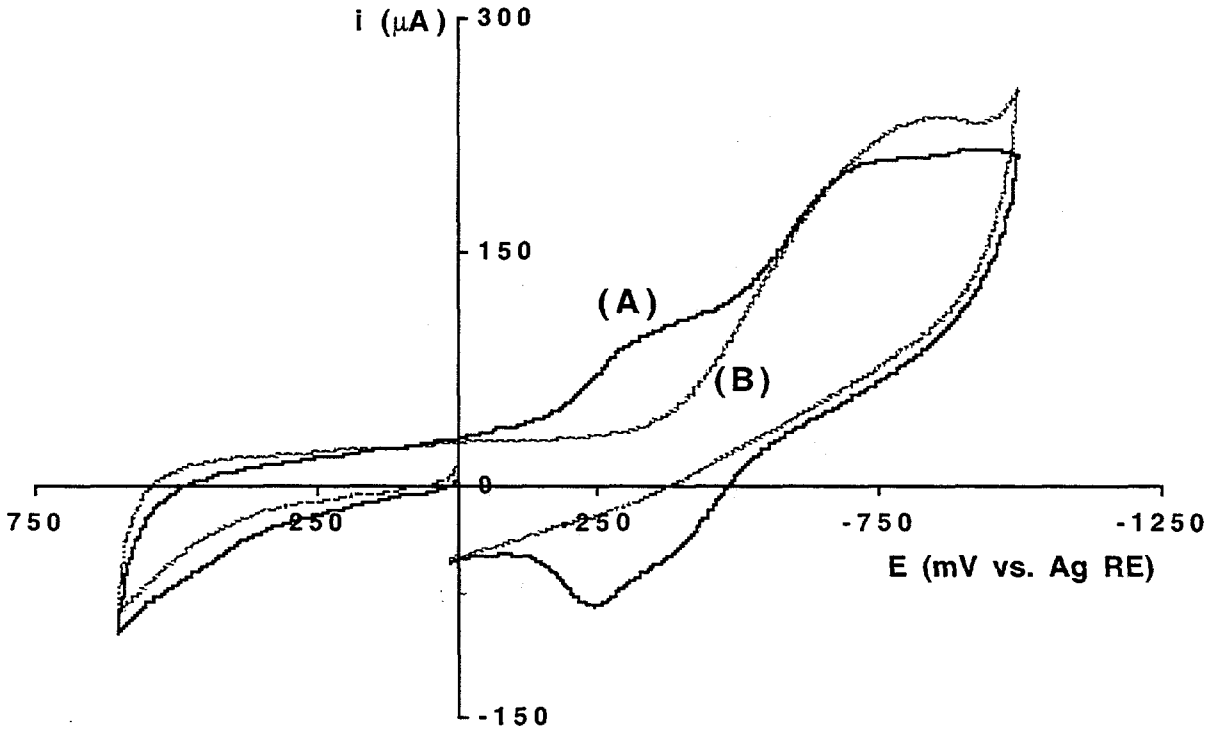

Figure 3. Cyclic voltammetry of Meldola's Blue in 0.1 M KNO_3, in the GLRS electrochemical cell (Figure 1b). Working electrode: Cr/fused silica diffraction grating coated with approximately 200 nm of semi-conformal gold. Dark curve (A) is 122 ppm Meldola's Blue. Light curve (B) is 0.1 M KNO_3 background. Initial potential: 0 mV vs. silver pseudo-reference electrode. Switching potentials: +600 and –1000 mV. Final potential: ~ 0 mV. Scan rate: 50 mV/sec.

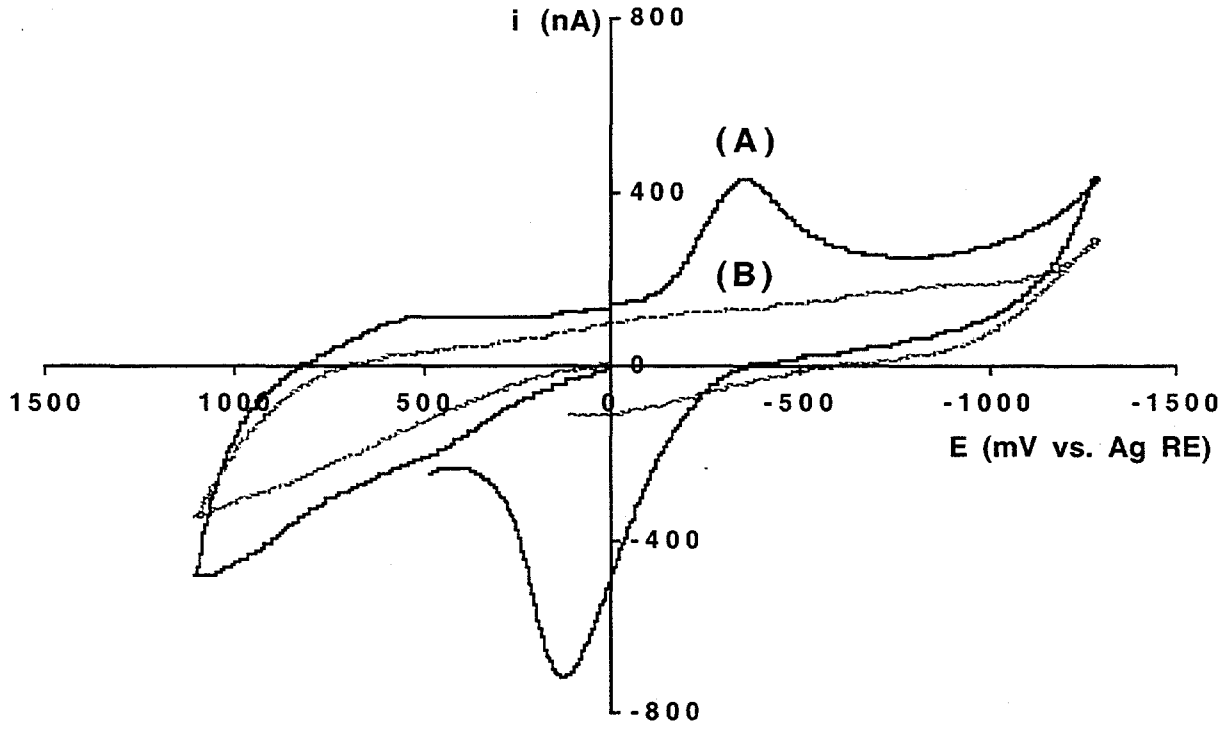

Figure 4. Cyclic voltammetry of Meldola's Blue in water, in a conventional electrochemical cell. Working electrode: 0.03 cm^2 Au disk. Dark curve (A) is 37 ppm Meldola's Blue. Light curve (B) is water background. Initial potential: 0 mV vs. silver pseudo-reference electrode. Switching potentials: +1100 and –1300 mV. Final potential: ~ +500 mV for Meldola's Blue, ~ + 100 mV for water. Scan rate: 50 mV/sec.

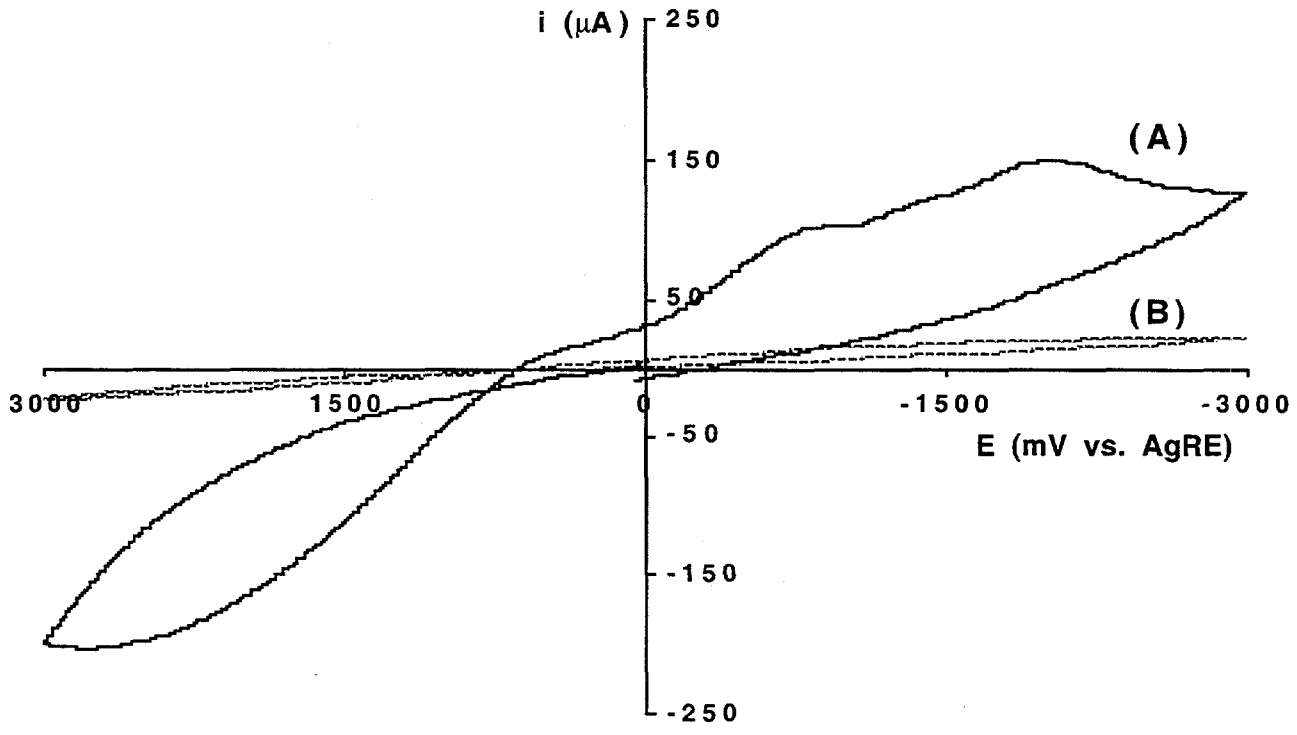

Figure 5. Cyclic voltammetry of Meldola's Blue in water, in the GLRS electrochemical cell (Figure 1b). Working electrode: Cr/fused silica diffraction grating coated with approximately 200 nm of semi-conformal gold. Dark curve (A) is 42 ppm Meldola's Blue. Light curve (B) is water background. Initial potential: 0 mV vs. silver pseudo-reference electrode. Switching potentials: +3000 and –3000 mV. Final potential: ~ 0 mV. Scan rate: 50 mV/sec.

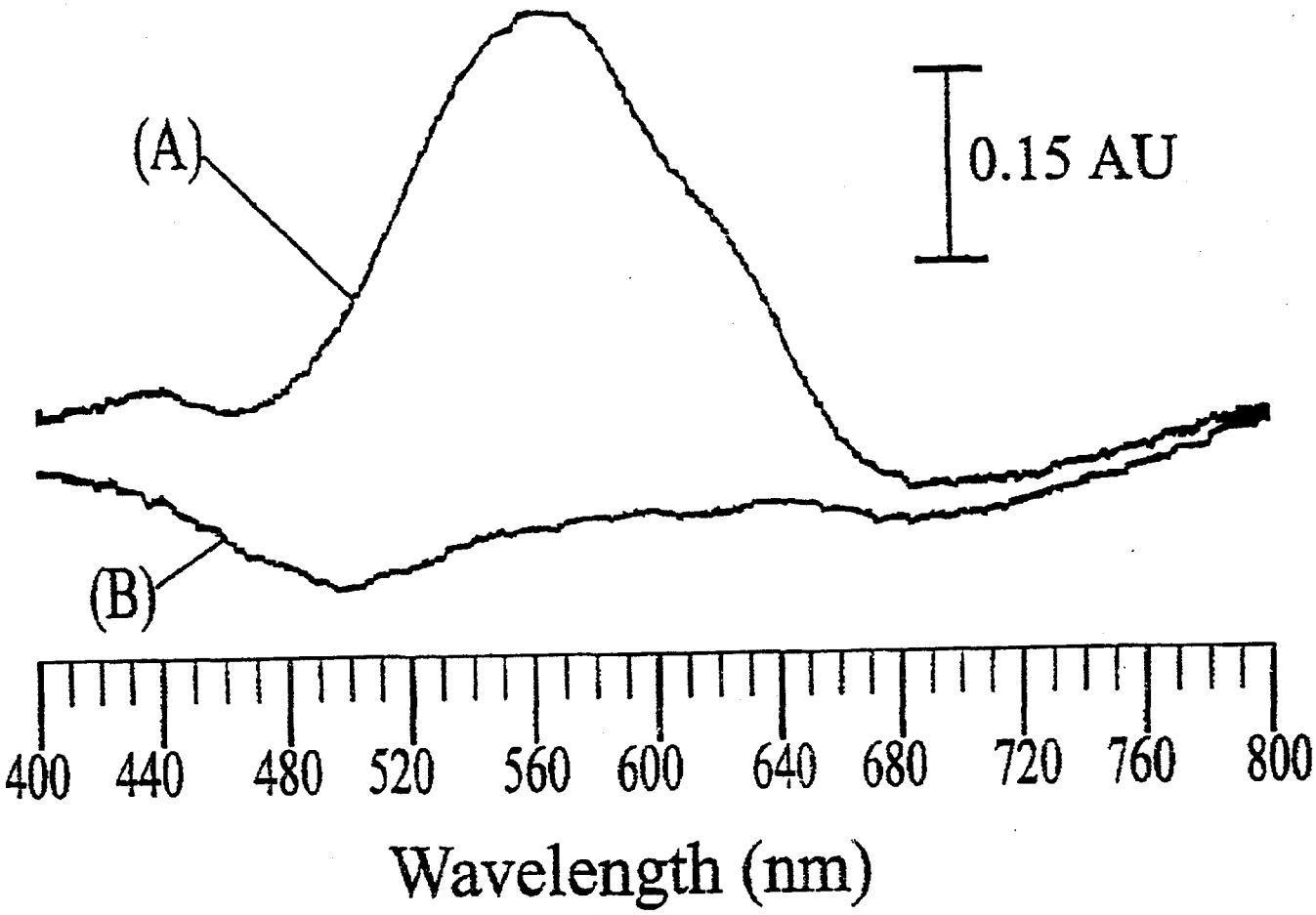

Figure 6. Visible absorbance spectra (in absorbance units, AU) obtained during thin layer potentiostatic reduction of 0.1 millimolar Meldola's Blue in a phosphate buffer (pH = 7.2). A spectroelectrochemical cell with a gold minigrid optically transparent thin layer electrode (OTTLE) was used. Applied potentials: (A) open circuit; (B) –200 mV vs. Ag/AgCl reference electrode. (From reference 13).

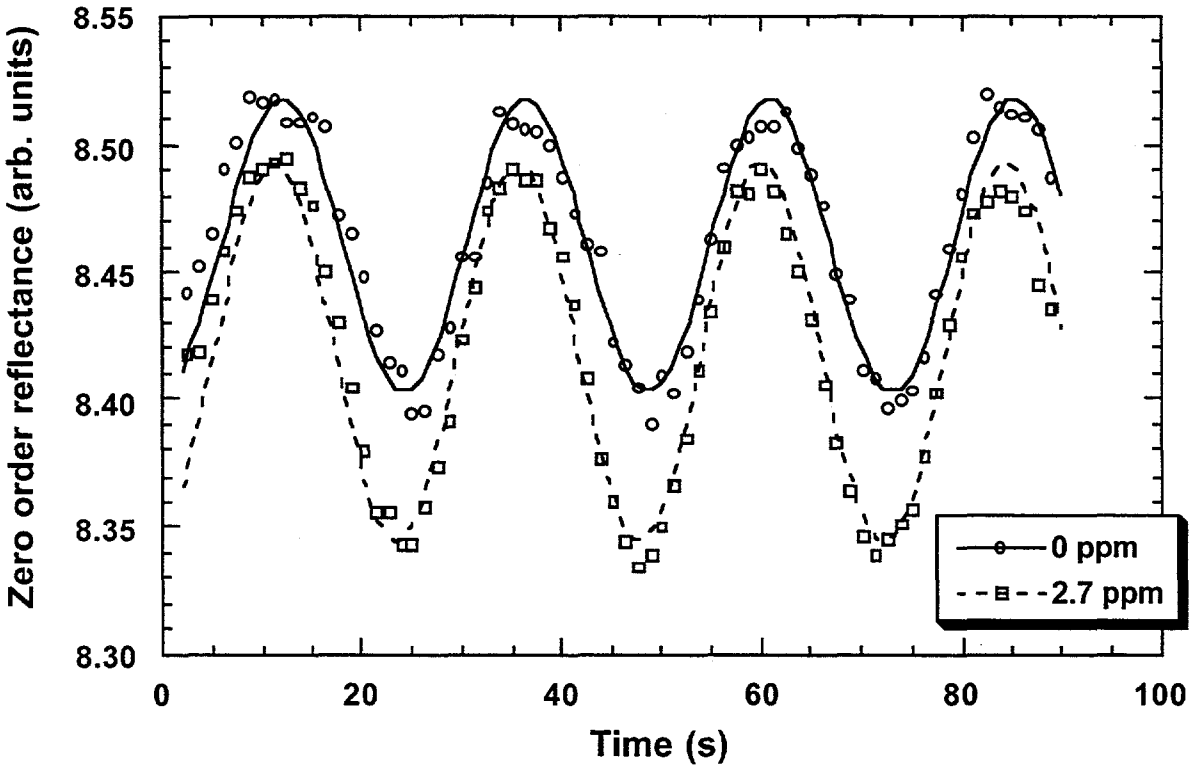

Figure 7. Zero order reflectance as a function of time for cyclic voltammetry experiments on a 2.7 ppm solution of Meldola's Blue in water (squares), as well as for pure water (circles). Working electrode (grating) was scanned between +3 and –3 volts (vs. Ag RE), scan rate = 500 mV/s, approximately 4 cycles. Experimental data are shown by symbols, sine curve fits are shown by solid or dashed curves.

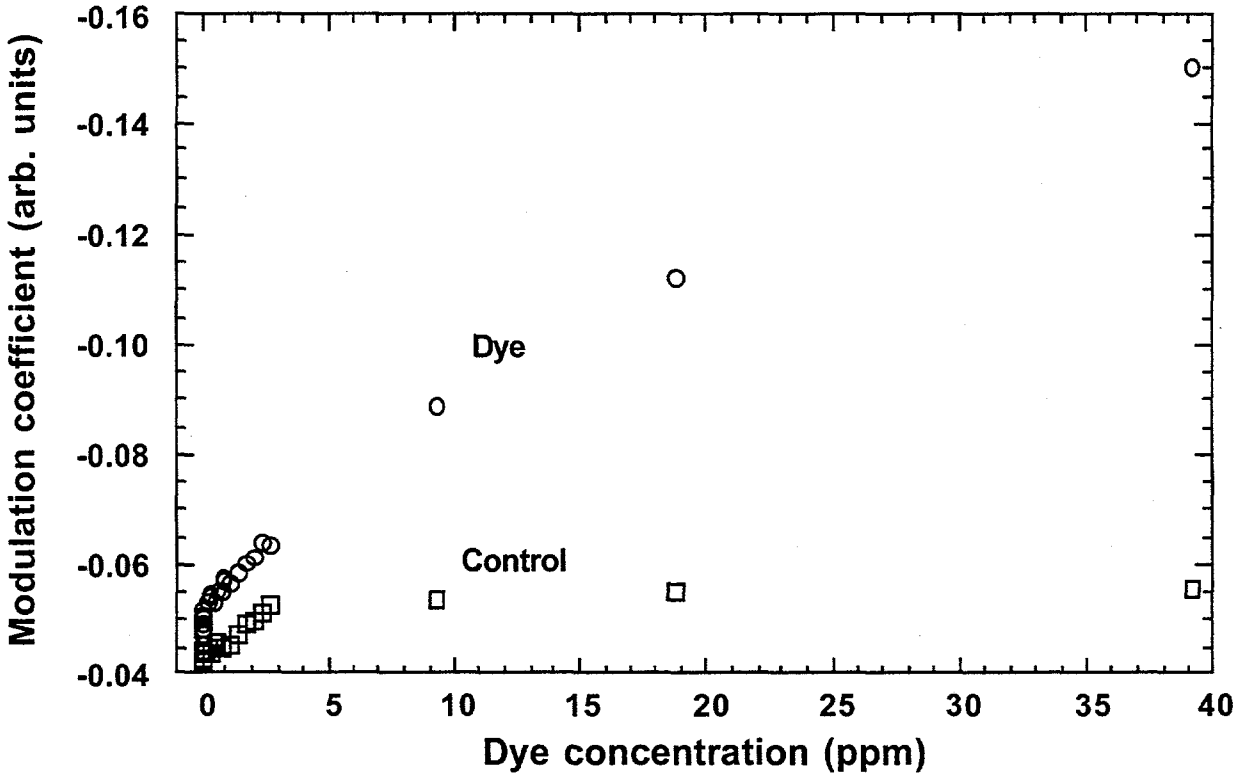

Figure 8. Modulation coefficient (m2 from Equation 4) as a function of Meldola's Blue dye concentration. The control experiment was conducted in an identical manner as the dye experiment, but in the absence of any added dye.

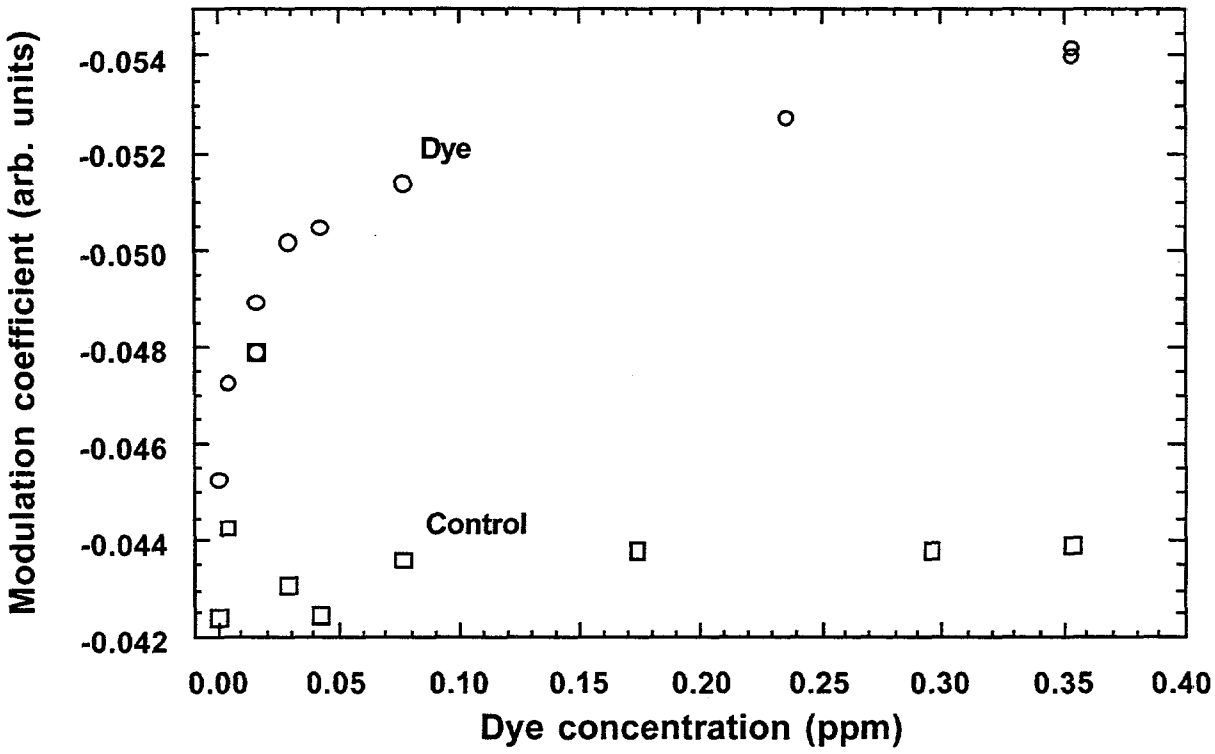

Figure 9. Expanded version of Figure 8. Modulation coefficient (m2 from Equation 4) as a function of Meldola's Blue dye concentration. The control experiment was conducted in an identical manner as the dye experiment, but in the absence of any added dye.

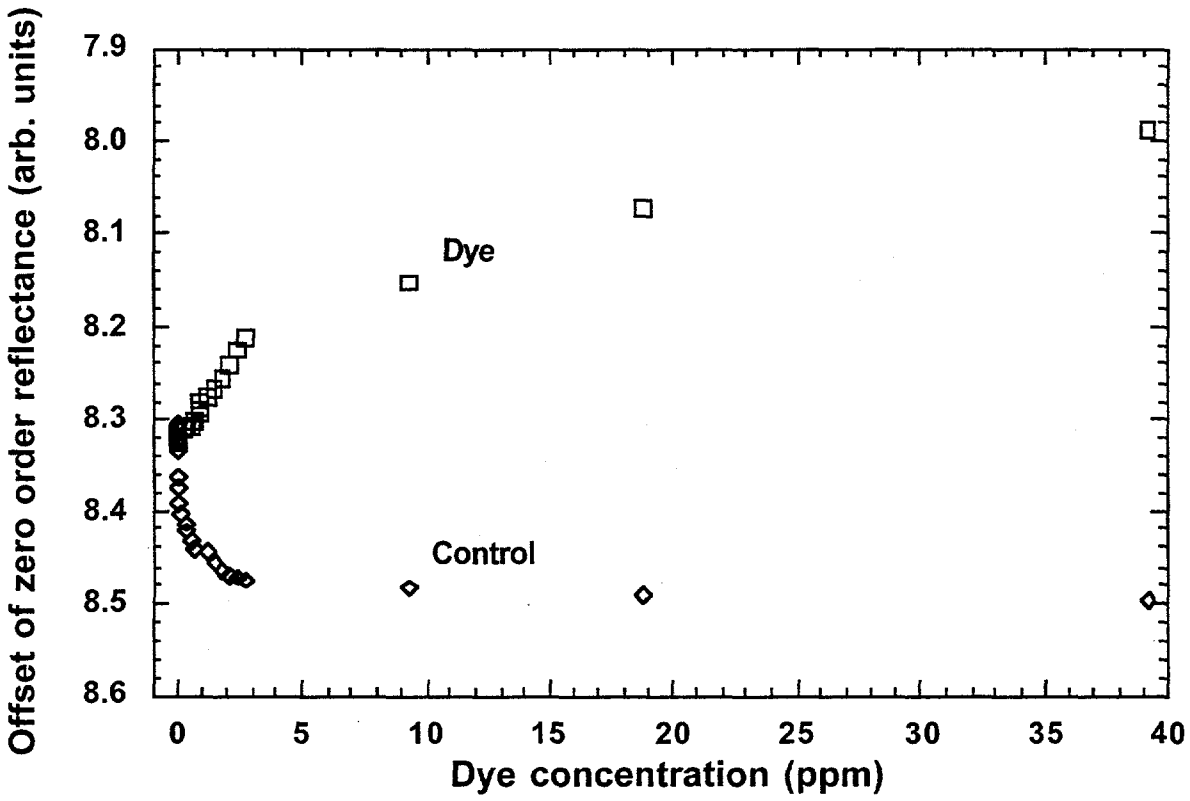

Figure 10. Offset of zero order reflectance (m1 from Equation 4) as a function of Meldola's Blue dye concentration. The control experiment was conducted in an identical manner as the dye experiment, but in the absence of any added dye.

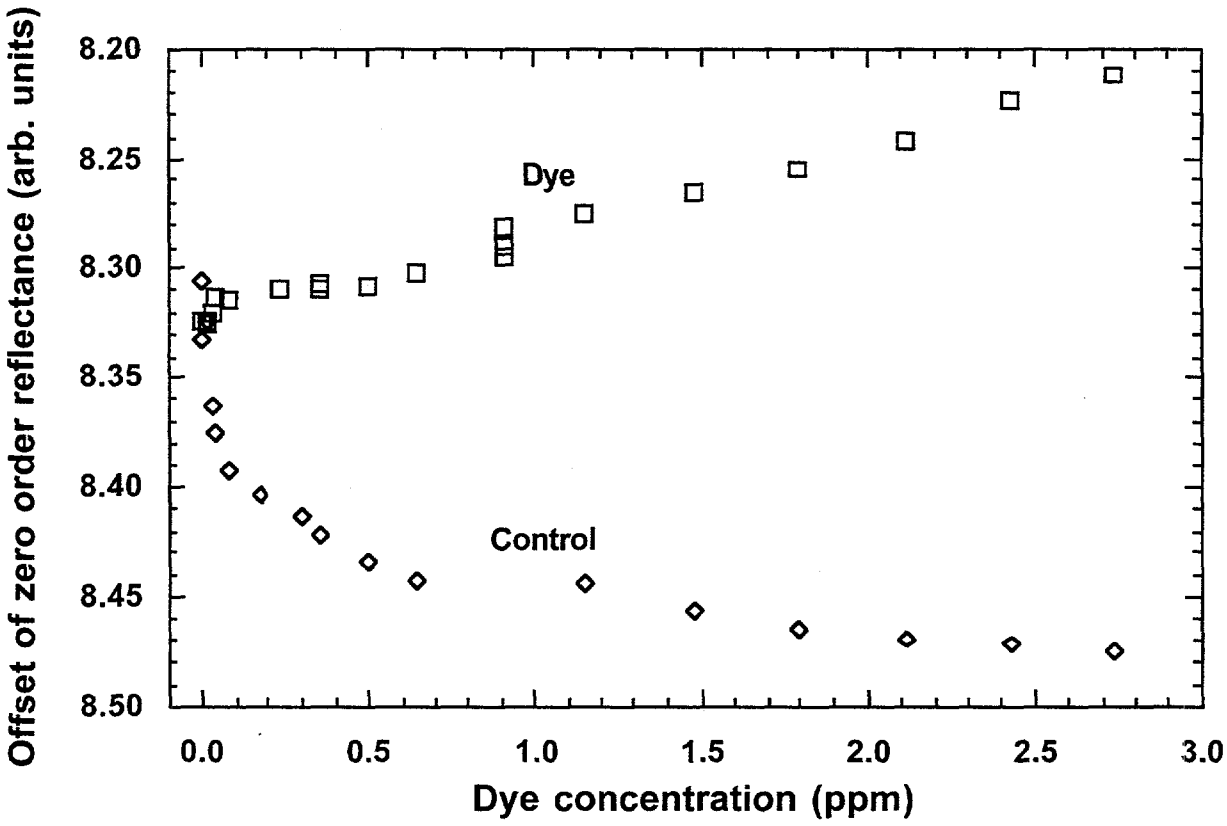

Figure 11. Expanded version of Figure 10. Offset of zero order reflectance (m1 from Equation 4) as a function of Meldola's Blue dye concentration. The control experiment was conducted in an identical manner as the dye experiment, but in the absence of any added dye.

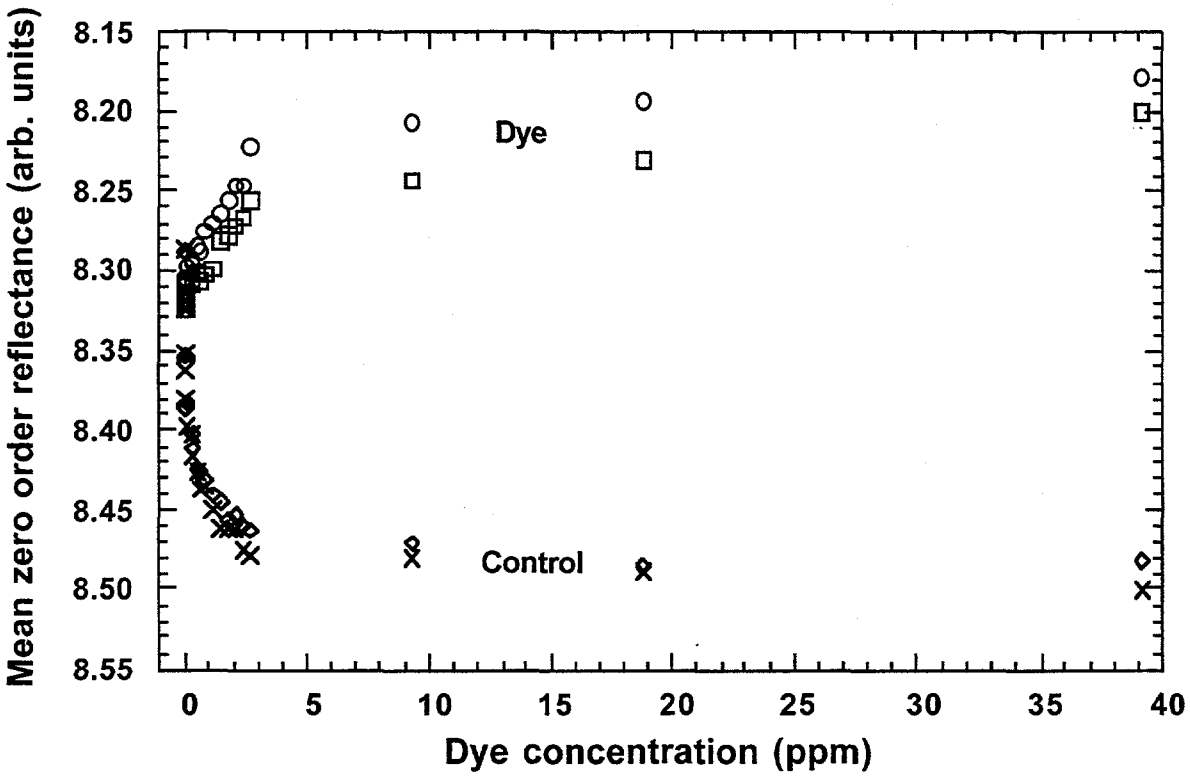

Figure 12. Zero order reflectance, as a function of Meldola's Blue dye concentration, in the absence of electrochemical modulation. For both the dye and the control experiments, the data was acquired immediately before (dye – open squares; control – x's) and immediately after (dye – open circles; control – open diamonds) the 4-cycle electrochemical modulation. Immediately before the electrochemical modulation, the grating was at rest potential. Immediately after the electrochemical modulation, the grating was in the process of returning to a rest potential from the final potential (+3 volts vs. Ag RE).

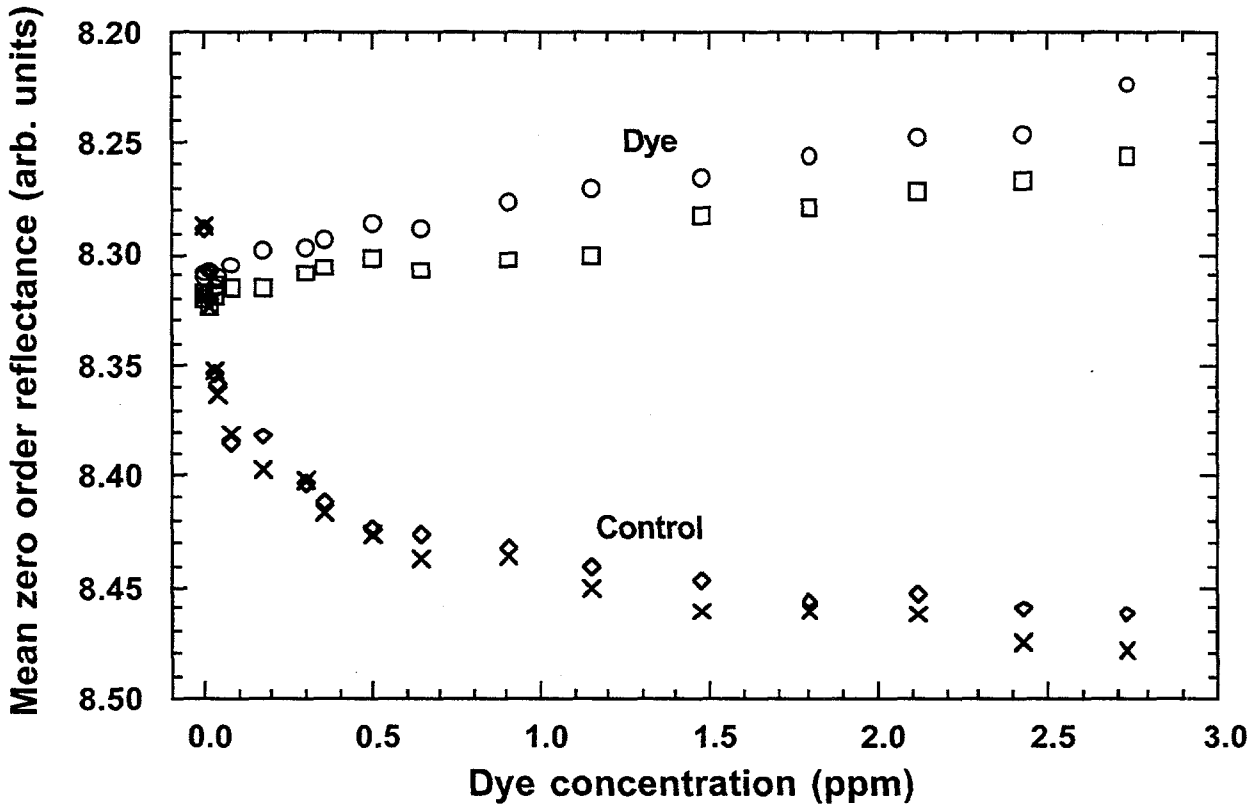

Figure 13. Expanded version of Figure 12. Zero order reflectance, as a function of Meldola's Blue dye concentration, in the absence of electrochemical modulation. For both the dye and the control experiments, the data was acquired immediately before (dye – open squares; control – x's) and immediately after (dye – open circles; control – open diamonds) the 4-cycle electrochemical modulation. Immediately before the electrochemical modulation, the grating was at rest potential. Immediately after the electrochemical modulation, the grating was in the process of returning to a rest potential from the final potential (+3 volts vs. Ag RE).

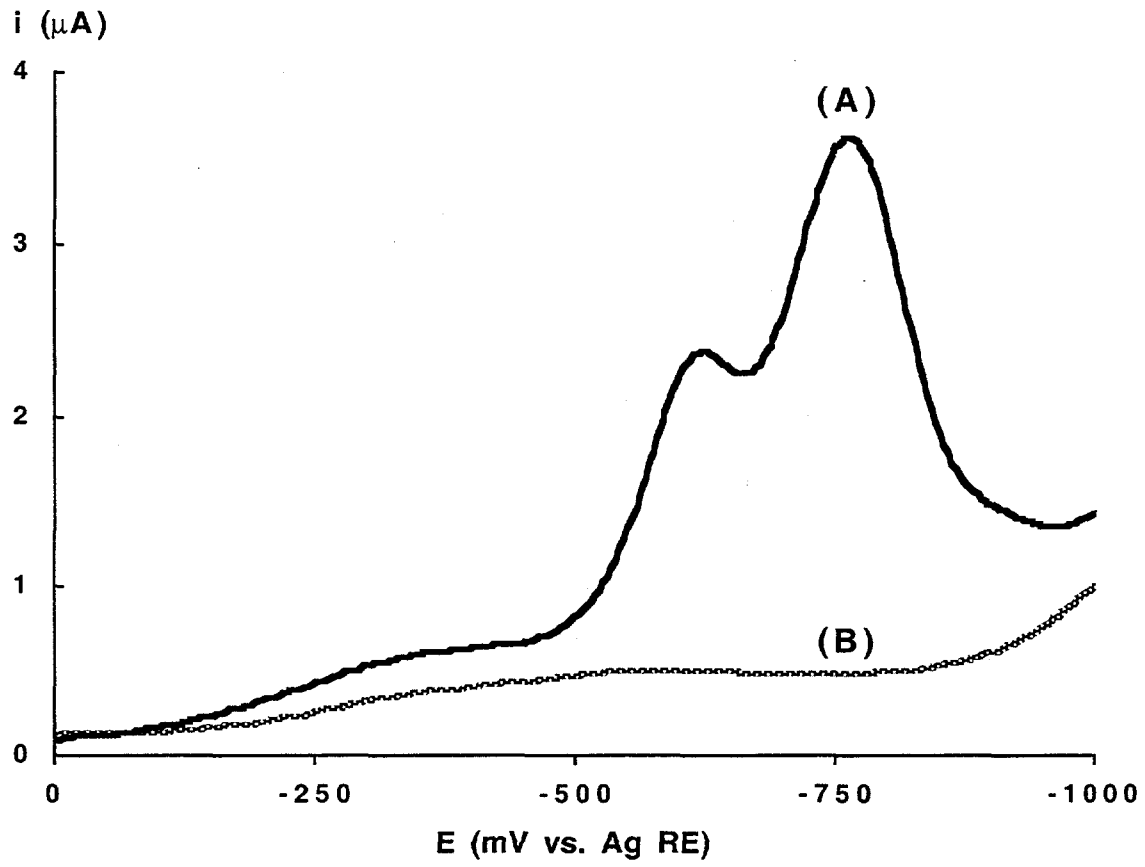

Figure 14. Osteryoung square wave voltammetry (OSWV) of TNT in 0.05 M KNO_3, in a conventional electrochemical cell. Working electrode: 0.03 cm^2 gold disk. Dark curve (A) is 45 ppm TNT. Light curve (B) is 0.05 M KNO_3 background. Initial potential: 0 mV vs. silver pseudo-reference electrode. Switching potential: -1000 mV. Square wave amplitude: 25 mV. Potential step amplitude: 4 mV. Frequency: 15 Hz.

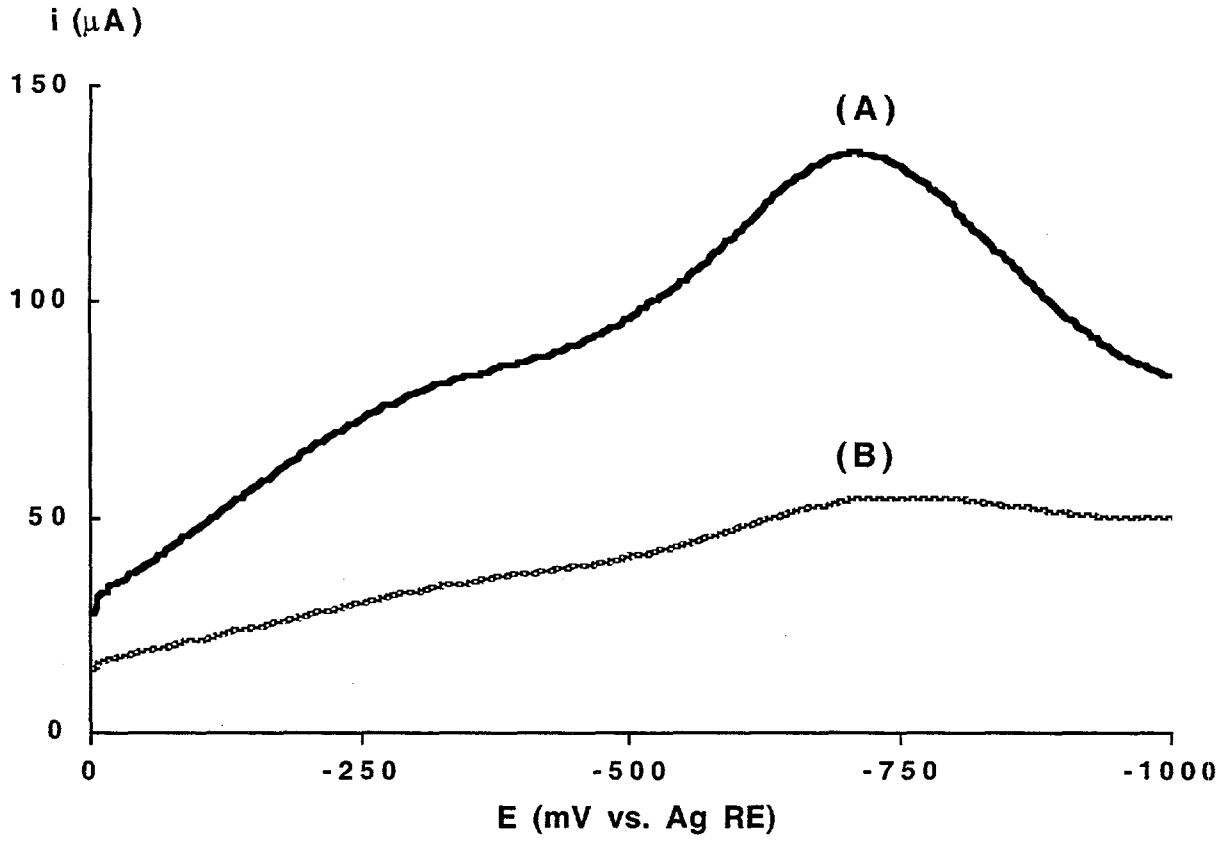

Figure 15. Osteryoung square wave voltammetry (OSWV) of TNT in 0.05 M KNO_3, in the GLRS electrochemical cell (Figure 1b). Working electrode: Chromium/fused silica diffraction grating coated with approximately 200 nm of semi-conformal gold. Dark curve (A) is 45 ppm TNT. Light curve (B) is 0.05 M KNO_3 background. Initial potential: 0 mV vs. silver pseudo-reference electrode. Switching potential: -1000 mV. Square wave amplitude: 25 mV. Potential step amplitude: 4 mV. Frequency: 15 Hz.

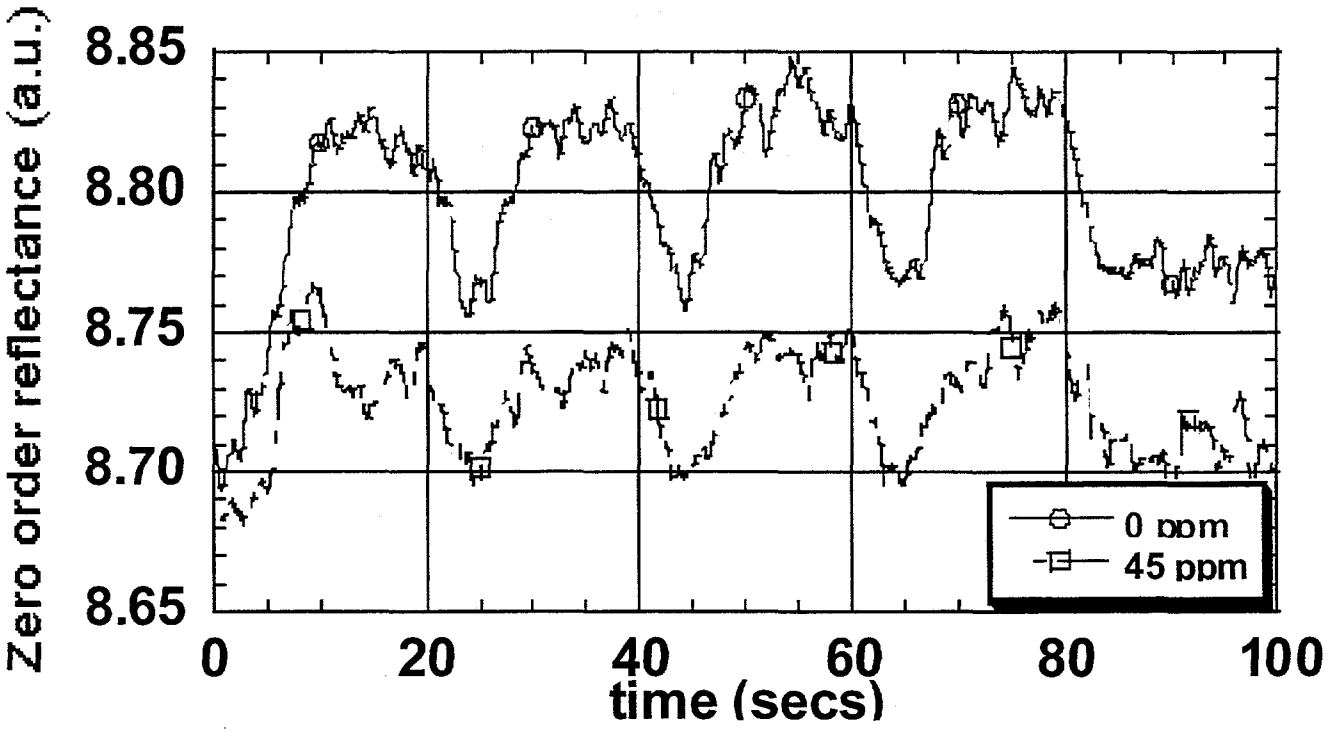

Figure 16. Zero order reflectance (arbitrary units, a.u.) as a function of time for cyclic voltammetry experiments on a 45 ppm solution of TNT in 0.05 M KNO_3 (squares), as well as for pure 0.05 M KNO_3 (circles). Working electrode was scanned between 0 and –1 volts (vs. Ag RE), scan rate = 100 mV/s, approximately 4 cycles.

Appendix - K. J. Kasunic, "Comparison of Kretschmann-Raether Angular Regimes for Measuring Changes in Bulk Refractive Index", *Applied Optics*, **39(1)**, 61-64 (2000).

Comparison of Kretschmann–Raether angular regimes for measuring changes in bulk refractive index

Keith J. Kasunic

We compare two angular regimes for the measurement of changes in the real refractive index of bulk fluid analytes. The measurements are based on the use of the Kretschmann–Raether configuration to sense a change in reflectivity with index. Specifically, we numerically simulate the relative sensitivities of the total internal reflection (TIR) and the surface-plasmon resonance (SPR) regimes. For a fixed-angle apparatus, the method that gives the greatest change in reflectivity varies with metal film thickness. For films thicker than the skin depth, the SPR regime is the most sensitive to index changes. For thinner films, however, the TIR angle is then dominant, with increases in sensitivity on the order of 75% for 10-nm gold or silver media.

OCIS codes: 120.0120, 120.5710, 260.6970, 240.6680.

1. Introduction

Two angular regimes for the measurement of changes in the real refractive index of fluid analytes may be classified as total internal reflective and surface-plasmon resonant. Perhaps the most common method is total internal reflection (TIR), found in many optical laboratories in the form of the Abbe refractometer.[1] This instrument utilizes the TIR that occurs at a high-to-low dielectric interface (e.g., prism-to-analyte), creating evanescent waves along the interface for a range of incident angles that depend on the ratio of indices. When referenced against a known prism index, the TIR technique can measure analyte index to an absolute accuracy of 1 part in 10^5. This accuracy is a result of experimental parameters such as prism flatness and angular resolution, rather than fundamental limitations.[2]

These same evanescent waves, when propagating along a metal–dielectric interface, can excite free-electron resonances called surface plasmons. This effect has been used in several device applications, typically as optical chemical sensors to measure changes in analyte contaminant concentration associated with changes in index.[3–11] Experimentally, surface-plasmon resonant (SPR) effects are observed as a sharp minimum in reflectivity as the angle of incidence is varied; as shown below, changes in the analyte index shift this minimum. By monitoring the resulting change in reflectivity at a fixed angle, one can then measure the change in analyte. As with TIR, variations in refractive index to 1 part in 10^5 have been measured with this technique.[5]

Our experiments, however, require the use of an electrode to excite the analyte electrically. Our design is also intended to measure index changes in a compact, portable device with the sensitivity of the Abbe refractometer. We are thus led to the Kretschmann–Raether configuration for plasmon excitation,[10] shown in Fig. 1. The experimental apparatus for measuring index changes with SPR are numerous.[10] The simplest approach is to measure the angular shift in reflectivity as the analyte is varied. For the case of SPR, the important feature to be monitored is the reflectivity minimum. The sensitivity is limited, however, because information contained in the slope of the reflectivity curve is ignored. Therefore a more useful approach is to select a fixed measurement angle and to obtain the change in reflectivity as index variations shift the reflectivity-versus-angle curve.[4–6,10] In this way, both the slope and the shift of the reflectivity curve are utilized.

Our goal is to evaluate the relative sensitivities of the TIR and the SPR regimes by use of the fixed-angle Kretschmann–Raether apparatus. We make no attempt to predict the limits on analyte index change that can be measured for each regime. Rather, we

When this research was performed, K. J. Kasunic (kasunic@u.arizona.edu) was with Sandia National Laboratories, Albuquerque, New Mexico 87185. He is currently with the Department of Mathematics, University of Arizona, Tucson, Arizona 85721.

Received 5 March 1999; revised manuscript received 7 June 1999.

0003-6935/00/010061-04$15.00/0

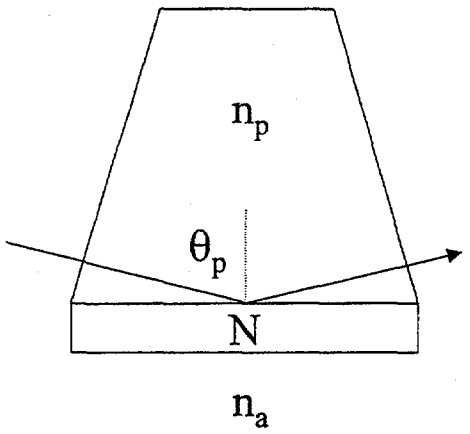

Fig. 1. Schematic of Kretschmann–Raether configuration for exciting surface plasmons. Prism with index n_p, metal film with index N, and analyte with index n_a.

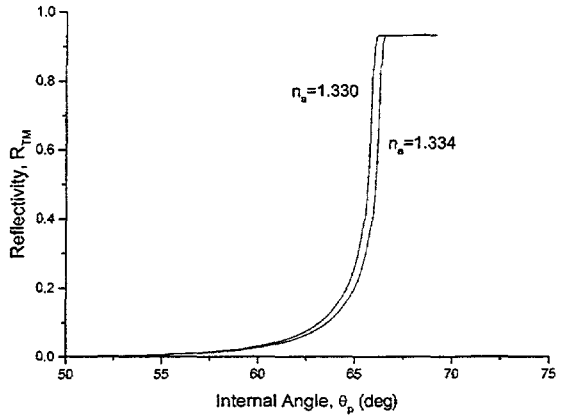

Fig. 2. Power reflectivity R_{TM} of TM-polarized field versus internal prism angle θ_p for the TIR method. The metal film thickness shown in Fig. 1 is zero. The prism index $n_p = 1.457$ at $\lambda = 0.633$ μm.

assume an index change and numerically simulate the change in reflectivity with the methods of Mansuripur.[12] Note that specific experimental parameters such as laser linewidth, manufacturing tolerances, temperature and dispersion compensation, etc. are not considered in our results. Also note that our calculations do not apply to the typical case of an adsorptive metal surface to which a thin film of a target species may adhere. Rather, we are concerned with measuring changes in bulk refractive index for which we assume a controlled analyte environment.

2. Theory

In this section, we briefly review the theory governing each of the two regimes. We start with the TIR method. As mentioned above, this common technique is the principle governing the Abbe refractometer, which can measure refractive indices to approximately 1 part in 10^5. Since our emphasis is on measuring changes in index as a measure of analyte contamination, we approach this method from a slightly different point of view. Specifically, to compare the sensitivity of TIR with SPR, we look at how the TIR (or critical) angle changes with analyte index. In the absence of a metal film, this angle is given by the familiar equation

$$\theta_{TIR} = \sin^{-1}(n_a/n_p), \tag{1}$$

where n_a and n_p are the (real) indices of the analyte and the prism, as shown in Fig. 1. An immediate disadvantage of this method is that the index of the prism must be larger than that of the analyte. A typical example of how the reflectivity varies with internal prism angle θ_p for a TM (or p-polarized) field is shown in Fig. 2.

The rationale for the Kretschmann–Raether SPR geometry is a phase matching of the incident field with free-electron (plasma) excitations at the metal–analyte surface. These surface plasmons have a wave number k_{sp} given by[7]

$$k_{sp} = \frac{\omega}{c}\,\mathrm{Re}\left[\frac{1}{\epsilon_a} + \frac{1}{\epsilon_m(\omega)}\right]^{-1/2}, \tag{2}$$

where ω is the frequency of the incident field, c is the speed of light in vacuum, ϵ_a $(=n_a^2)$ is the dielectric constant of the analyte, and $\epsilon_m(\omega)$ is the complex dielectric constant of the metal. For phase matching to occur, k_{sp} must equal k_x, the x component of the wave number of the incident light in the prism

$$k_x = \omega n_p \sin\theta_p/c. \tag{3}$$

Note that Eqs. (2) and (3) are readily solved for the angle at which a reflection minimum occurs, known as the surface-plasmon angle θ_{sp}. This angle depends on n_a, thus providing the basis for the SPR technique.

For free electrons at long wavelengths away from the bulk plasma frequency ω_p, the frequency dependence of $\epsilon_m(\omega)$ is given by[10]

$$\epsilon_m(\omega) = 1 - \frac{\omega_p^2}{\omega^2}. \tag{4}$$

Substituting this result in Eq. (2), we obtain a plasmon dispersion equation for $\omega(k_{sp})$, with a frequency that asymptotically approaches $\omega_p/(1+\epsilon_a)^{1/2}$ for large k_{sp}. Graphically, the phase matching needed for surface plasmons is found from the intersection of this asymptotic curve with the straight line given by Eq. (3). This cannot occur unless the slope of Eq. (3) is less than that of the asymptotic curve at the origin (see, for example, Ref. 7, Fig. 3), easily shown to be c/n_a. This compares with a slope of $c/n_p \sin\theta_p$ for the prism dispersion. The two slopes are equal when $\sin\theta_p = n_a/n_p$, which is identical to the TIR condition given by Eq. (1). Surface plasmons can therefore only be generated by evanescent waves. Also note the importance of the prism index; the SPR

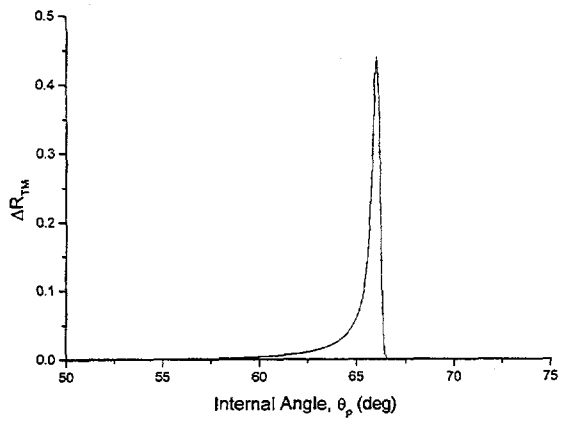

Fig. 3. Change in reflectivity ΔR_{TM} versus θ_p for the conditions of Fig. 2.

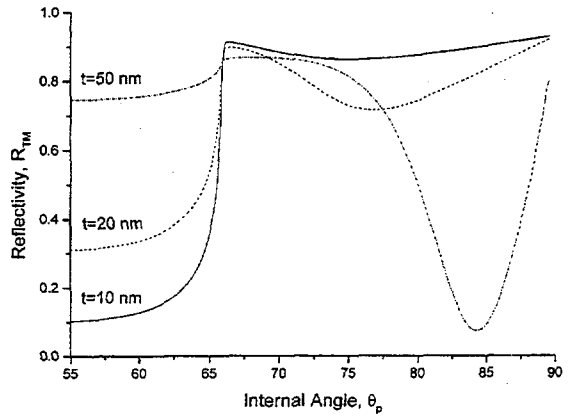

Fig. 4. Reflectivity R_{TM} versus θ_p for the SPR method. The metal film is gold with a complex index $N_g = 0.13 + i\,3.16$. The prism index is the same as in Fig. 2; the analyte index is $n_a = 1.330$.

technique thus suffers from the same disadvantage as the TIR.

3. Numerical Results and Discussion

In this section, we present numerical results comparing the sensitivity of each of the two regimes to changes in analyte index. Our modeling is based on Diffract,[12] a commercially available physical-optics software package. TIR results are shown in Fig. 2, where we plot the TM reflectivity R_{TM} as a function of internal prism angle θ_p. The figure assumes a prism index $n_p = 1.457$ for fused silica at $\lambda = 0.633$ μm and bulk analyte indices of n_a equal to 1.330 and 1.334. Neglecting Fresnel losses at the entrance to the prism, the results show the well-known approach to a reflectivity of unity as θ_p approaches the TIR condition $\theta_{TIR} \approx 65.9°$, given by Eq. (1). Both the slope of this curve near the TIR angle and the shift with index indicates the change in reflectivity ΔR_{TM}. This is quantified in Fig. 3, which shows the plot of the angular dependence of ΔR_{TM} for the given $\Delta n_a = 0.004$. The figure clearly illustrates the greatest sensitivity to index changes near the critical angle.

For the SPR regime, we take 10 nm as a practical lower limit on film thickness.[13] Figure 4 shows how R_{TM} for the Kretschmann–Raether arrangement varies with θ_p for gold films of thickness t equal to 10, 20, and 50 nm. For clarity, we plot the curves for only 1 index ($n_a = 1.330$). The significant features of this curve are twofold. As discussed above, SPR requires an evanescent angle $\theta_{sp} > \theta_{TIR}$. Up to a point, these effects are enhanced for the thicker metallic films, with 50 nm yielding an approximately optimum response for gold. However, the thicker films also reduce the sensitivity of the TIR effect, as the reflectivity is large for angles less than θ_{TIR} for a film thickness approaching the skin depth δ of the metal (≈32 nm for the assumed complex index $N_g = 0.13 + i\,3.16$ for gold).[14] This is illustrated in Fig. 5, which shows the plot of ΔR_{TM} for $\Delta n_a = 0.004$. The results clearly show the greater sensitivity to analyte changes near the TIR angle for the 10-nm film; alternatively, the SPR regime dominates for the 50-nm film. Comparing the two sensitivities for the assumed prism, electrode, and analyte indices, we see that the critical angle has approximately 75% greater sensitivity than the SPR angle for a 10-nm gold film. Additional simulations show that a detection scheme with a sensitivity of 1% is required for measuring a bulk index change $\Delta n_a = 10^{-5}$ near the TIR angle for a 10-nm gold film, whereas a sensitivity of 0.2% is required for the SPR regime.

This is further illustrated in Fig. 6, which shows the plot of $\Delta R_{TM,max}$ as a function of film thickness for the TIR and the SPR angles. That is, for each thickness, we obtain ΔR_{TM} versus θ_p for the conditions of Fig. 3 in 0.1° increments. We then record the maximum value of ΔR_{TM} near both angles. The resulting plot clearly illustrates the transition from a SPR-dominated sensitivity for $t \geq \delta$, to a TIR-dominated response for thinner films. We have also modeled a silver film as the plasma medium ($N_s = 0.27 + i\,4.18$), obtaining almost identical results. In addi-

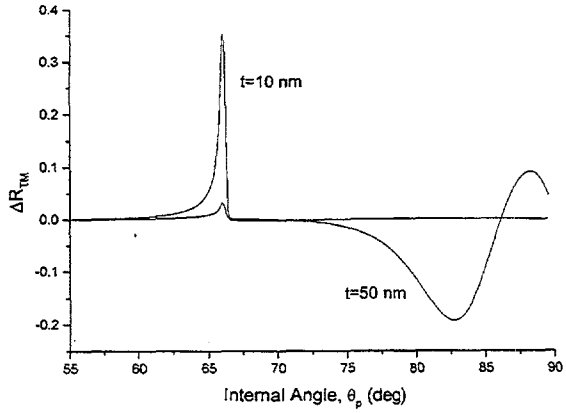

Fig. 5. Change in reflectivity ΔR_{TM} versus θ_p for the conditions of Fig. 4.

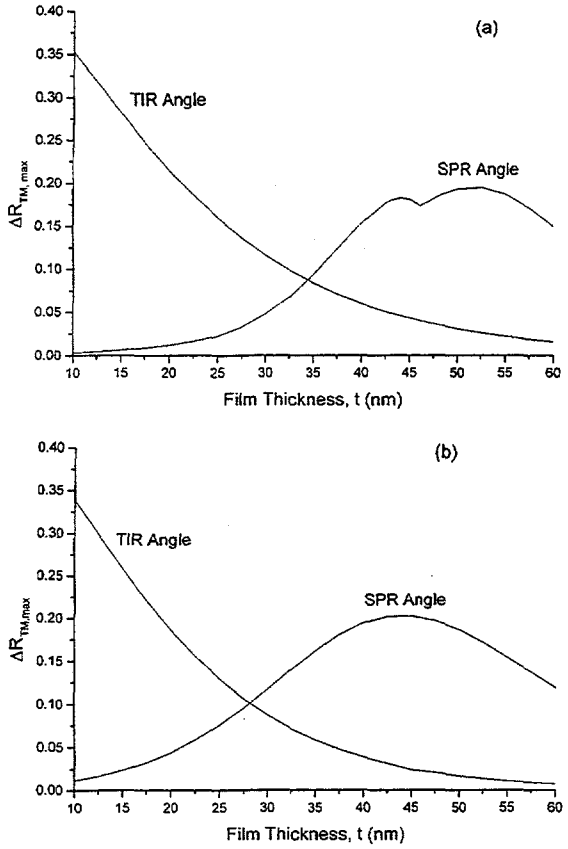

Fig. 6. Maximum reflectivity change $\Delta R_{TM,max}$ as a function of film thickness for the conditions of Fig. 4. (a) Gold film results, where the skin depth δ_g is approximately 32 nm. (b) Silver results, where δ_s is 24 nm.

tion, for the same percentage change in index (n_a = 1.000 and 1.003), our simulations with a gas as the analyte fluid show similar features, though to a much smaller degree.

4. Conclusions

We have compared two angular regimes for the measurement of changes in the real refractive index of bulk fluid analytes. For a fixed-angle apparatus, the method that gives the greatest change in reflectivity varies with metal film thickness. For films thicker than the skin depth, the SPR regime is the most sensitive to index changes. For thinner films, however, the TIR angle is then dominant, with increases in sensitivity on the order of 75% for 10-nm gold or silver media. Specific experimental parameters such as laser linewidth, temperature and dispersion compensation, manufacturing tolerances on film thickness, etc. were not accounted for in our results. Including these effects may therefore modify these conclusions. Nevertheless, the potential for measuring bulk index changes in a compact, portable device with the same sensitivity as the Abbe refractometer should prove an effective impetus for further research in this area.

The author appreciates useful discussions with M. Kelly and S. Kemme of Sandia National Laboratories; M. Descour, L. Li, and M. Mansuripur of the University of Arizona; S. Zaidi of the University of New Mexico; and J. Turner-Valle of Ball Aerospace.

References

1. F. Jenkins and H. White, *Fundamentals of Optics*, 4th ed. (McGraw-Hill, New York, 1976), p. 27.
2. D. Tentori and C. L. Famozo, "High-accuracy critical angle refractometry," Opt. Eng. **32,** 593–601 (1993).
3. H. Raether, "Surface plasma oscillations and their applications," in *Physics of Thin Films*, G. Hass, M. Francombe, and R. Hoffman, eds. (Academic, New York, 1977), Vol. 9, Chap. 3.
4. C. Nylander, B. Liedberg, and T. Lind, "Gas detection by means of surface plasmon resonance," Sens. Actuators **3,** 79–88 (1982/83).
5. B. Liedberg, C. Nylander, and I. Lundstrom, "Surface plasmon resonance for gas detection and biosensing," Sens. Actuators **4,** 299–304 (1983).
6. P. Daniels, J. Deacon, M. Eddowes, and D. Pedley, "Surface plasmon resonance applied to immunosensing," Sens. Actuators **15,** 11–18 (1988).
7. K. Matsubara, S. Kawata, and S. Minami, "Optical chemical sensor based on surface plasmon measurement," Appl. Opt. **27,** 1160–1163 (1988).
8. L. Zhang and D. Uttamchandani, "Optical chemical sensing using surface plasmon resonance," Electron. Lett. **24,** 1469–1470 (1988).
9. G. J. Sprokel and J. D. Swalen, "The attenuated total reflection method," in *Handbook of Optical Constants of Solids*, E. Palik ed. (Academic, New York, 1991), Chap. 4.
10. K. Welford, "Surface plasmon-polaritons and their uses," Opt. Quantum Electron. **23,** 1–27 (1991).
11. N. Peyghambarian, S. Koch, and A. Mysyrowicz, *Introduction to Semiconductor Optics* (Prentice Hall, Englewood Cliffs, N.J., 1993), Sec. 3.6.
12. M. Mansuripur, "Analysis of multilayer thin-film structures containing magneto-optic and anisotropic media at oblique incidence using 2 × 2 matrices," J. Appl. Phys. **67,** 6466–6475 (1990).
13. A. E. Craig, G. A. Olson, and D. Sarid, "Experimental observation of the long-range surface-plasmon polariton," Opt. Lett. 8, 380–382 (1983).
14. D. R. Lide, *CRC Handbook of Chemistry and Physics*, 77th ed. (CRC Press, Boca Raton Fla., 1996), pp. 12–126.

Distribution

1	MS0603	M. E. Warren, 1743
1	MS0603	W. C. Sweatt, 1743
1	MS0603	S. A. Kemme, 1743
1	MS1405	G. V. Herrera, 1812
10	MS0343	M. J. Kelly, 1812
1	MS0188	D. L. Chavez, 4001 (LDRD program office)
1	MS1085	M. H. Florez, 7400-1
1	MS0415	K. J. Almquist, 9811
1	MS0415	D. S. Blair, 9811
1	MS9018	Central Technical Files, 8940-2
2	MS0899	Technical Library, 9616
1	MS0612	Review & Approval Desk, 9612, For DOE/OSTI